Inversion of moment tensor focal mechanisms for active stresses around the Microcontinent Iberia: Tectonic implications

de Vicente, G.; Cloetingh, S.A.P.L.; Munoz-Martin, A.; Olaiz, A.; Stich, D.; Vegas, R.; Galindo-Zaldivar, J.; Fernandez-Lozano, J.

published in
Tectonics
2008

DOI (link to publisher)
10.1029/2006TC002093

document version
Publisher's PDF, also known as Version of record

Inversion of moment tensor focal mechanisms for active stresses around the microcontinent Iberia: Tectonic implications

G. de Vicente,[1] S. Cloetingh,[2] A. Muñoz-Martín,[1] A. Olaiz,[1] D. Stich,[3] R. Vegas,[1] J. Galindo-Zaldívar,[4] and J. Fernández-Lozano[1]

Received 14 December 2006; revised 15 July 2007; accepted 16 October 2007; published 7 February 2008.

[1] The Iberian microcontinent and its connected oceanic crust are affected by deformations related to the Eurasian-African plate boundary. Active stress inversions from populations of moment tensor focal mechanisms have been performed around and inside the Iberian peninsula, using a total of 213 moment tensor estimates. Main results are as follows: (1) The tensorial solutions show better consistency and lower misfits compared to those obtained previously from first P arrival focal mechanisms. (2) Along the Eurasia-Africa western boundary, the type of active stresses progressively changes easternward from triaxial extension to uniaxial compression along the Terceira Ridge, the Gloria Fault zone, and the Gulf of Cadiz. (3) In the Betics-Alboran-Rif zone, uniaxial extension predominates with S_{hmax} N155°E trending. (4) In northern Algeria, uniaxial compression reappears. (5) The Iberian foreland is currently under strike-slip to uniaxial extension tensorial conditions. **Citation:** de Vicente, G., S. Cloetingh, A. Muñoz-Martín, A. Olaiz, D. Stich, R. Vegas, J. Galindo-Zaldívar, and J. Fernández-Lozano (2008), Inversion of moment tensor focal mechanisms for active stresses around the microcontinent Iberia: Tectonic implications, *Tectonics*, *27*, TC1009, doi:10.1029/2006TC002093.

1. Introduction and Tectonic Setting

[2] The Iberian Peninsula is located in an area of NW-SE "slow" convergence (~3 to 6 mm/a, depending on longitude) between two larger plates, Eurasia and Africa [e.g., *DeMets et al.*, 1990; *Calais et al.*, 2003; *McClusky et al.*, 2003; *Serpelloni et al.*, 2008]. The Azores-Gibraltar fracture area has marked the westernmost portion of the plate boundary since the Lower Miocene (cron 6c, 24 Ma), when the Iberian Plate came to form part of Eurasia [*Srivastava et al.*, 1990]. During the Cenozoic, its paleogeographic and tectonic evolution was related to the Alpine Orogeny and to the closing of the Tethys Ocean [*Savostin et al.*, 1986; *Ziegler*, 1988; *Dewey et al.*, 1989; *Andeweg*, 2002; *Jabaloy et al.*, 2002].

[3] The relative movements between Iberia, Eurasia and Africa have conditioned the tectonic evolution of their limits, although recent data point to an intense mechanical coupling between Iberia and Africa during good part of the Tertiary [*Vegas et al.*, 2005]. The most recent tectonic events (Pyrenean and Betic orogenies) can be explained starting from the kinematic reconstructions carried out by *Srivastava et al.* [1990] and *Roest and Srivastava* [1991] for the Cretaceous to the Upper Oligocene and by *Mazzoli and Helman* [1994] for this period to the present time. During most part of the Cretaceous, the Iberian Plate was independent. From the Upper Cretaceous until the Upper Eocene (84–42 Ma, cron 34–42), it formed part of the African plate. The Africa-Eurasia limit extended from the Bay of Biscay to the Pyrenees (Figure 1a). In the westernmost sectors, the initial displacement was divergent and progressively changed to strike-slip, while in the Cantabrian margin there was subduction of oceanic crust, and in the Pyrenees the continental collision begins [*Ziegler*, 1988]. In this way, the triple point between North America–Eurasia-Africa changed from Ridge-Ridge-Ridge (RRR) to Ridge-Ridge-Fault (RRF).

[4] From the Upper Eocene to the Lower Miocene (42–24 Ma, cron 18-6c), the Iberian Plate moved again independently along the King Trough–Pyrenees to the north and along the Azores-Gibraltar fault to the south. In the King Trough oceanic expansion took place, while in the Pyrenean area the compressional maximum was reached (with a NNW-SSE shortening orientation) during the Upper Eocene. The Azores-Gibraltar fracture area had a small relative movement until the Lower Oligocene (cron 13, 36 Ma) and since then the regime has been extension near Azores, strike-slip in the Gloria Fault and compressional to the east of the Gorringe Bank. In the Lower Miocene, the Africa-Eurasia limit became active (Figures 1c, 1d, 2 and 3). The direction of convergence changed several times over the Neogene: NNE from the Upper Oligocene to the Burdigalian (25.5–16.2 Ma, anomalies 7-5C), NNW from the Langhian to the lower Tortonian (16.2–8.9 Ma, anomalies 5C-5) and NW from the Upper Tortonian until today (8.9–0 Ma, anomaly 5 to the present time). A similar tectonic

[1]Grupo de Investigación en Tectonofísica Aplicada, Departamento Geodinámica, Universidad Complutense de Madrid, Madrid, Spain.
[2]Faculty of Earth and Life Sciences, Vrije Universiteit Amsterdam, Amsterdam, Netherlands.
[3]Sezione di Bologna, Istituto Nazionale di Geofisica e Vulcanologia, Bologna, Italy.
[4]Departamento Geodinámica, Universidad de Granada, Granada, Spain.

0278-7407/08/2006TC002093$12.00

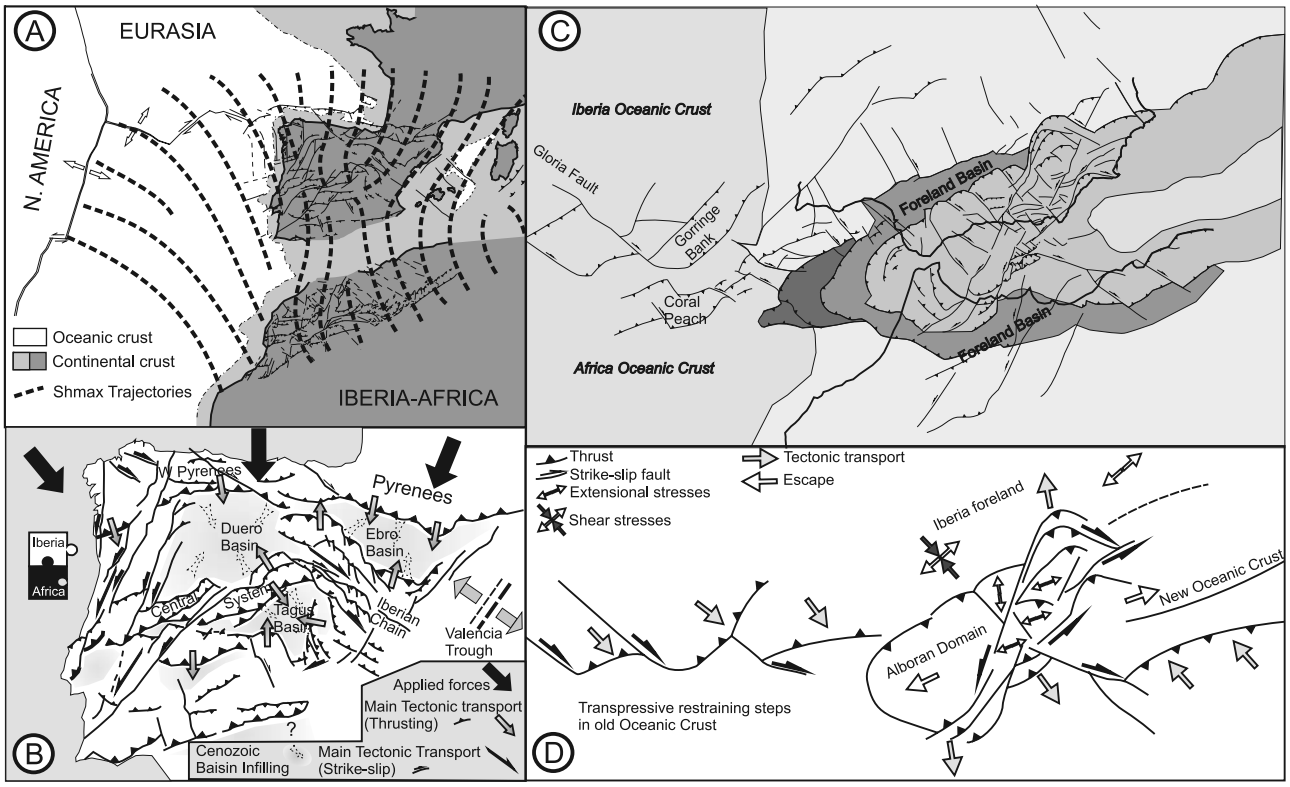

Figure 1. Tectonic sketches of the Microcontinent Iberia. (a) Paleostresses distribution during the Oligocene–Lower Miocene. Constrictive conditions of the deformation prevail on the Iberia interior [*de Vicente et al.*, 2006]. (b) Applied forces, main active structures and tectonic transports during the Oligocene–Lower Miocene. (c) Tectonic map of the Gulf of Cadiz–Betics-Alboran-Rif-Tell zone. Not all the drawn features have been active at the same time. (d) Tectonic interpretation of Figure 1c up to the Upper Miocene to explain the tectonic escape of the Alboran Domain [*Vegas*, 1992].

configuration to the current one was already reached in the Upper Miocene [*de Vicente*, 2004] (Figures 1b–1d).

2. Active Stresses Around Iberia

[5] In the present situation, the distribution of earthquake epicenters defines a net contact between the Eurasian and the North American Plates, and a more diffuse one toward the African Plate and inside the Iberian Peninsula (Figure 2). Hypocentral depths are generally shallow in young oceanic crust at the Mid-Atlantic Ridge and near the Azores triple point, but maximum focal depths increase eastward along the Eurasia-Africa plate contact, including populations of intermediate deep events (~40–130 km) in the Gulf of Cadiz and Alboran Sea. Occasional very deep focus events (~600–650 km) occur under Southern Iberia [*Grimison and Chen*, 1986; *Buforn et al.*, 1990; *Morales et al.*, 1999; *Stich et al.*, 2005a].

[6] The analysis of earthquakes focal mechanisms by means of inversion methods allows determining the state of active stresses in the two plate limits [*Consejo de Seguridad Nuclear*, 1998; *de Vicente et al.*, 2000; *Herraiz et al.*, 2000; *de Vicente et al.*, 2006; *Stich et al.*, 2006]. The Mid-Atlantic Ridge represents the divergent limit between the North American–Eurasia and North American–African plates, and its active structures are normal faults. To the north of the Azores triple point, the Ridge has a N-S orientation and produces a push toward N96E. To the south of the triple point, it pushes toward N114E [*de Vicente et al.*, 2000]. The Ridge is divided in sectors that are limited by transform faults where important deflections in the shortening direction occur.

[7] The seismicity in the limit between the Eurasian-African Plates defines four different geodynamic sectors, from the Azores triple point up to the Iberian Peninsula [*Grimison and Chen*, 1986; *Buforn et al.*, 1988; *Kiratzi and Papazachos*, 1995]: an area of oceanic divergence in the Terceira Ridge, an intraoceanic transformant area, a zone of oceanic convergence and an area of continental convergence. The Azores islands, aligned according to a NW-SE trend and with an active vulcanism, are the surface expression of the Terceira Ridge. As in the Mid-Atlantic Ridge, the main structures are extensional and, in this case, they accommodate an extension toward N42E. From the south end of the Terceira Ridge up to an approximate longitude of 10°W, an intraoceanic transformant zone appears that is characterized by the absence of instrumentally recorded seismicity in its westernmost part, the Gloria fault (Figures 1 and 3). To the

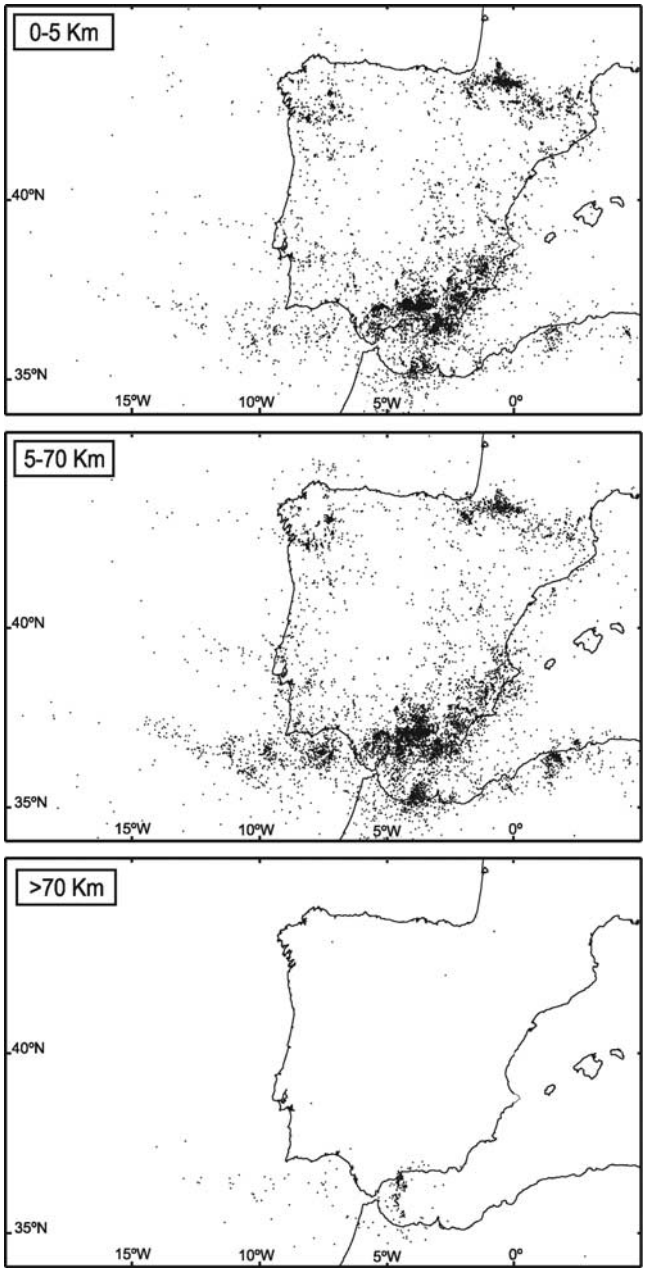

Figure 2. Distribution of epicenters in Western Eurasia–Africa limit. (top) Hypocentral depth between 0 and 30 km. (middle) Hypocentral depth higher than 30 km. (bottom) Hypocentral depth higher than 70 km.

east, an oceanic area is located with a complex bathymetry [*Vázquez and Vegas*, 2000] where the orientation of the active structures is quite heterogeneous and the stress-strain regime changes progressively from pure strike-slip to transpressive deformation [*Sartori et al.*, 1994; *Zitellini et al.*, 2004], with an orientation of the maximum horizontal stress (S_{hmax}) toward N145E. Finally, near the contact between the Iberian southern margin and the African continent, the area of continental convergence is located within a diffuse distribution of earthquake epicenters (Figure 2).

[8] This NW-SE and NNW-SSE orientation of S_{hmax} is also characteristic of Western Europe, where the stress regime is compressional to strike-slip [*Rebaï et al.*, 1992; *Müller et al.*, 1992; *Zoback*, 1992]. This trend, seemingly uniform in the stress trajectories, has important deviations in certain regions related with first-order faults and crustal heterogeneities. The regional pattern [*Zoback*, 1992] is conditioned by the driver forces of the movement of the tectonic plates, concretely the push of the Mid-Atlantic Ridge and the collisional forces in the convergent Eurasia-Africa limit [*Zoback et al.*, 1989; *Müller et al.*, 1992; *Grünthal and Stromeyer*, 1992]. However, numeric models of intraplate stresses in Europe obtain results that are more in agreement with the observed data when other sources of stresses like lateral density variations are also included [*Gölke and Coblentz*, 1996; *Andeweg*, 2002]. These kinematic models have also contributed to the improvement of the knowledge on the magnitude range of active tectonic stresses [*Engelder*, 1993], at around 10–20 MPa on average in a 100 km thickness lithosphere [*Gölke and Coblentz*, 1996].

[9] Detailed works indicate that most of the Iberian Peninsula is under a NW-SE S_{hmax} (strike-slip regime) that has stayed practically constant since the Upper Miocene [*Galindo-Zaldívar et al.*, 1993; *de Vicente et al.*, 1996; *Ribeiro et al.*, 1996; *Herraiz et al.*, 2000; *de Vicente et al.*, 2000]. Toward the NE part of the Peninsula, a bending of the stress trajectories takes place, and S_{hmax} becomes N-S and NE-SW, which affects the Pyrenees, the Ebro Basin and the Valencia Trough (Figure 1) [*Consejo de Seguridad Nuclear*, 1998; *Jurado and Müller*, 1997; *Schindler et al.*, 1998; *Goula et al.*, 1999; *Herraiz et al.*, 2000; *de Vicente et al.*, 2000]. Concerning this strike-slip environment, it is necessary to highlight the coexistence of zones with an extensive regime, like the Iberian Chain and the Valencia Trough [*Consejo de Seguridad Nuclear*, 1998; *Schindler et al.*, 1998; *de Vicente et al.*, 2000; *Herraiz et al.*, 2000].

3. Moment Tensor Focal Mechanisms

[10] The direction of slip, along a fault plane during an earthquake, responds to the stress conditions at the source location. Thus earthquakes sample the present-day tectonic stress field over the entire thickness of the seismogenic layer. Therefore earthquake focal mechanisms are valuable and widely used stress indicators, and several stress field studies for the region have been based on 'first motion' focal mechanisms, estimates derived from the spatial pattern of observed first arrival polarities over the recording network [*Consejo de Seguridad Nuclear*, 1998; *Herraiz et al.*, 2000]. With the densification of the seismic broadband network in recent years, regional moment tensor inversion has become an alternative to first motion techniques and is now systematically applied to regional seismicity [*Pondrelli et al.*, 2002, 2004, *Braunmiller et al.*, 2002; *Stich et al.*, 2003; *Rueda and Mezcua*, 2005]. These moment tensor projects invert three-component time domain displacement

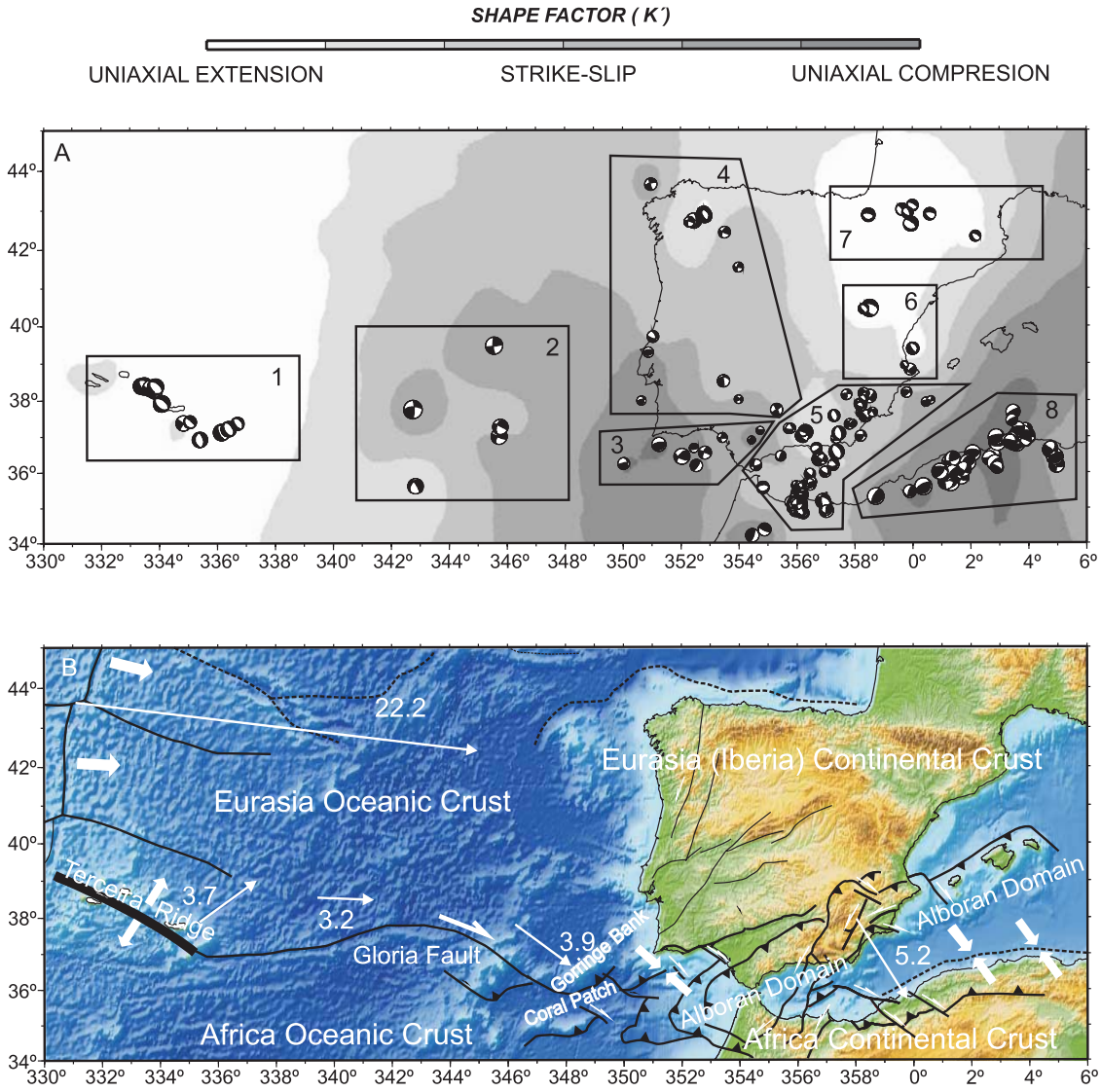

Figure 3. (a) Type of strain ellipsoid distribution (scaled K values, see text for explanation), analyzed focal mechanisms, and selected zones where stress inversion has been carried out: 1, Terceira Ridge; 2, Gloria Fault; 3, Gulf of Cadiz; 4, Western Iberia; 5, Central-Eastern Betics, Alboran Sea, and Rif; 6, Iberian Chain; 7, Pyrenees; and 8, northern Algeria. (b) Main tectonic features of the Western Eurasia–Africa limit. Thin white arrows give local plate velocities of Eurasia relative to North America and Africa (Nubia), based on model NUVEL1A [*DeMets et al.*, 1990].

seismograms, including P-, S- and surface waves, for the mechanical force system associated with earthquake slip, thereby combining a far more complete evaluation of the recorded wavefield with a more general parameterization of the seismic source. The consideration of the full phase and amplitude information of several wave groups helps to constrain the source orientation, and moment tensor solutions can be obtained from relatively few regional recordings [e.g., *Dreger and Helmberger*, 1993; *Randall et al.*, 1995]. In this way, moment tensor inversion can be applied to a relevant number of events, contributing to a better spatial sampling and larger populations of focal mechanisms. Simultaneously, full waveform inversion can overcome ambiguities in traditional first motion solutions. The 1999 Mula earthquake (SE-Spain) is a good example: While the first motion pattern is equally consistent with reverse and strike-slip faulting [*Buforn et al.*, 2005], full waveform inversion can exclude the reverse solution owing to basic incompatibilities with surface wave observations [*Mancilla et al.*, 2002].

[11] Moment tensor solutions for the western Eurasia-Africa limit are available from several routine moment tensor projects: The global Harvard centroid moment tensor (CMT) catalogue [*Dziewonski and Woodhouse*, 1983] contains events larger than magnitude ~5.5 since 1977; this catalogue contributes solutions mainly for northern Algeria

Table 1. Focal Mechanisms Database[a]

Longitude	Latitude	Depth	S1*	D1**	R1***	S2*	D2**	R2***	Sc	Iexp	Name	Catalog
					Terceira Ridge (1)							
−26.65	38.37	15	326	69	−78	115	24	−119	116	23	000304	ETH
−26.64	38.41	15	335	44	−87	151	46	−92	575	23	970628B	HRV
−26.52	38.4	15	301	35	−111	145	57	−76	743	24	970627A	HRV
−26.27	38.34	15	345	29	−37	109	73	−114	715	24	881121D	HRV
−26.16	38.26	15	284	27	−147	164	76	−67	622	23	970627B	HRV
−26.13	38.38	15	141	42	−80	307	49	−99	318	24	810212A	HRV
−25.92	37.92	15	131	41	−87	307	50	−93	345	24	890121A	HRV
−25.92	37.92	15	131	41	−87	307	50	−93	345	24	890121A	HRV
−25.16	37.38	15	303	90	180	33	90	0	889	23	881016A	HRV
−24.94	37.42	4	306	73	−97	149	18	−68	442	22	010213	ETH
−2.46	36.93	12	178	37	−79	345	54	−98	954	23	840909B	HRV
−23.85	37.13	15	319	28	−106	157	63	−82	375	24	960309G	HRV
−23.61	37.22	15	330	45	−90	150	45	−90	817	23	911209C	HRV
−2.33	37.37	6	145	56	−87	320	34	−95	707	22	000605	ETH
					Gloria Fault (2)							
−17.16	35.62	15	217	37	−28	330	74	−123	135	24	790112B	HRV
−14.44	39.48	32	173	78	4	82	86	168	852	24	830124C	HRV
−17.25	37.75	10	265	64	167	1	78	26	454	25	831017B	HRV
−14.27	37.01	10	206	69	8	113	82	158	186	24	060110	ETH
−14.23	37.27	14	199	49	−12	297	80	−138	115	24	060109	ETH
					Gulf of Cadiz (3)							
−8.76	36.78	50	57	25	70	259	67	99	21	23	861020	IAG
−7.17	36.55	30	203	71	−3	294	86	−161	55	22	880725	IAG
−7.97	36.45	6	220	64	26	117	67	151	16	24	000705	IAG
−7.47	36.19	6	35	75	90	217	15	91	375	22	021210	IAG
−6.57	36.97	60	189	70	9	96	82	160	106	21	030718	IAG
−5.56	36.9	6	29	40	82	219	51	96	191	20	030725A	IAG
−9.98	36.25	8	257	83	119	360	30	15	187	22	041213	IAG
−7.55	36.68	30	79	68	111	212	30	48	897	20	050103	IAG
−5.27	37.16	4	273	68	58	152	38	143	142	20	020915	IAG
					Western Iberia (4)							
−6.01	38.02	20	315	76	177	46	87	14	431	20	050220	IAG
−8.96	39.72	16	348	51	−38	105	61	−134	11	22	990430	IAG
−9.36	37.99	20	255	72	132	4	46	26	614	20	020328	IAG
−6	41.53	10	277	78	−179	187	89	−11	634	20	030112A	IAG
−6.01	41.54	12	102	88	165	192	75	2	217	21	030123	IAG
−4.7	37.74	12	58	86	−176	327	86	−3	208	21	030124	IAG
−6.53	38.52	36	353	89	50	262	40	178	378	22	060122	IGN
−9.11	39.3	18	264	50	104	63	42	74	224	21	060415	IGN
−6.48	42.44	21	116	86	15	208	63	4	16	22	060610	IGN
					Betics-Alboran-Rif (5)							
−3.86	35.51	8	137	59	−173	43	84	−30	45	22	881005	IAG
−3.91	35.37	15	112	48	−173	17	85	−42	101	24	940526D	HRV
−3.78	34.84	6	116	54	−118	338	44	−56	79	21	981020	IAG
−4.1	35.24	10	118	83	−149	24	59	−7	88	21	990718	IAG
−5.17	35.58	10	263	55	−88	81	35	−92	28	22	990804	IAG
−3.55	35.95	14	130	75	−138	27	49	−18	63	21	000813	IAG
−3.72	35.63	6	212	71	−53	325	40	−150	749	20	001128	IAG
−3.72	35.63	6	212	71	−53	325	40	−150	75	21	001128	IAG
−3.93	35.5	8	128	71	−157	30	68	−20	95	21	010608A	IAG
−4.03	35.63	14	132	55	−143	19	61	−40	619	20	020627A	IAG
−3.92	35.63	18	132	52	−135	11	57	−47	192	20	020706	IAG
−3.83	35.58	12	124	67	−171	30	81	−23	95	20	030215	IAG
−3.55	35.67	4	56	72	15	321	76	161	203	22	030218A	IAG
−3.61	35.67	2	81	72	49	331	44	153	419	20	030218B	IAG
−3.49	35.73	4	60	45	14	320	80	134	121	21	030219	IAG
−3.6	35.69	2	135	89	−136	43	46	−1	419	20	030221A	IAG
−3.62	35.69	4	48	51	0	138	90	−141	249	21	030221B	IAG
−3.55	35.7	4	245	88	44	153	46	177	419	20	030222	IAG
−4	35.14	14	11	72	−17	107	73	−161	288	24	040224	IAG
−4.08	35.17	16	123	67	−148	19	61	−26	329	21	040224	IAG
−4.08	35.05	10	11	68	−7	104	83	−157	169	21	040224	IAG
−3.91	35.07	10	106	49	−173	12	85	−40	126	21	040224	IAG
−3.95	35.11	16	97	74	−165	3	76	−15	106	21	040224	IAG

Table 1. (continued)

Longitude	Latitude	Depth	S1*	D1**	R1***	S2*	D2**	R2***	Sc	Iexp	Name	Catalog
−3.93	35.12	14	0	69	−4	92	86	−158	473	21	040225	IAG
−3.86	35.05	10	108	73	−167	14	77	−16	691	22	040225	IAG
−3.94	35.17	10	117	73	−162	22	73	−16	11	21	040225	IAG
−4.06	35.19	16	13	75	−9	105	80	−165	245	21	040226	IAG
−3.99	35.13	14	102	71	−170	8	81	−19	404	21	040227	IAG
−3.96	35.13	12	10	73	−5	102	84	−163	313	21	040227	IAG
−3.92	35.18	14	110	80	−163	16	74	−10	622	21	040227	IAG
−4.01	35.02	4	36	35	23	287	77	123	236	21	040228	IAG
−3.87	35.15	6	198	89	29	108	61	179	378	22	040302	IGN
−3.99	35.17	12	102	82	171	193	81	8	487	21	040304	IGN
−4.01	35.06	22	93	81	−171	2	81	−8	316	22	040307	IAG
−3.89	35.12	33	189	84	16	98	74	174	219	21	040307	IGN
−4.08	34.91	6	354	68	−50	109	44	−148	114	21	040310	IAG
−4.05	34.92	6	352	49	−62	134	47	−118	22	22	040312	IAG
−4.2	35.11	12	119	54	−148	9	65	−39	717	20	040315	IAG
−4.22	35.17	9	73	50	120	210	48	59	836	21	040318	IGN
−4.15	35	10	119	56	−164	20	77	−34	734	21	040320	IAG
−4.1	35.09	8	28	53	14	289	79	142	133	21	040401	IAG
−4.11	35.06	6	110	33	160	216	79	59	238	21	040406	IAG
−4.02	35.16	24	99	77	165	193	75	14	448	21	040523	IGN
−3.88	34.94	6	122	47	−131	355	57	−54	293	21	040620	IAG
−4.07	35.16	6	358	62	−46	115	50	−141	382	20	040710	IAG
−3.89	34.87	6	129	60	−115	352	38	−53	504	21	040814	IAG
−3.98	35.1	9	176	86	4	85	86	176	902	21	041010	IGN
−2.98	34.92	15	184	65	−17	282	74	−154	26	23	041202A	ING
−3.1	35.19	15	285	46	−151	174	70	−47	554	23	041204A	ING
−2.98	34.93	6	87	37	169	186	84	53	406	21	050322	ING
−5.42	36.21	8	178	61	−159	78	72	−30	17	22	880708	IAG
−3.7	37.12	6	166	27	−78	333	64	−96	39	23	840624	IAG
−2.63	36.57	20	335	43	−88	152	47	−92	851	23	931223A	HVR
−1.63	37.57	10	44	35	−7	140	86	−125	459	22	960902	IAG
−3.71	37.15	12	200	30	−35	323	73	−115	85	21	961228	IAG
−3.83	37.02	16	302	86	−89	120	4	−92	28	22	970224	IAG
−3.24	36.35	8	135	63	−178	44	88	−26	61	22	970702A	IAG
−3.26	36.37	10	131	73	−167	38	78	−17	46	22	970702B	IAG
−3.24	36.37	6	134	68	−165	38	76	−22	99	21	970702C	IAG
−3.24	36.45	16	212	82	20	119	70	172	28	21	970807	IAG
−3.02	36.01	4	117	71	−133	8	47	−25	64	21	971013	IAG
−1.79	37.01	8	21	58	17	282	76	147	89	21	980406	IAG
−4.26	37.22	14	335	55	−19	77	73	−143	25	21	980413A	IAG
−4.28	37.22	14	346	61	−20	87	72	−150	24	21	980413B	IAG
−4.21	37.22	12	88	69	−145	344	58	−25	18	21	980414A	IAG
−2.64	36.95	20	85	54	131	209	53	48	27	21	981016	IAG
−2.1	38.21	8	42	66	34	297	59	152	38	21	981114	IAG
−3.79	36.99	8	134	66	−62	263	35	−135	15	22	981118	IAG
−1.49	38.11	6	41	69	−25	141	66	−157	17	23	990202	IAG
−2.74	36.21	6	327	49	−35	83	63	−133	78	21	990529	IAG
−2.17	37.34	8	18	88	41	287	49	177	44	21	990614A	IAG
−2.74	36.21	6	327	49	−35	83	63	−133	727	21	990614B	IAG
−1.69	38.18	6	331	57	−169	235	81	−33	508	21	990814	IAG
−3.13	36.36	16	30	78	−12	123	77	−167	31	21	000527	IAG
−1.77	37.66	4	54	62	102	210	30	70	44	21	000802	IAG
−1.63	37.57	10	44	35	−7	140	86	−125	13	22	000823A	IAG
−2.28	38.15	8	270	73	170	3	81	18	44	21	010716	IAG
4.6	37.95	4	49	26	57	265	68	105	845	20	011206	IAG
−2.55	37.09	10	166	33	−92	348	57	−88	14	23	020204	IAG
−1.84	37.9	8	119	68	−140	11	53	−27	347	21	020806	IAG
−1.83	37.9	6	115	73	−122	0	35	−28	881	20	020806	IAG
−1.82	37.85	6	120	74	−124	7	37	−27	234	20	020807	IAG
−1.84	37.87	6	130	70	−122	11	37	−33	108	20	020807	IAG
−4.56	36.46	70	96	21	165	201	85	70	242	21	020824	IAG
−1.82	37.87	3	273	84	134	9	44	8	229	21	030409	IGN
6.3	38	14	12	85	−13	103	77	−175	155	20	030720A	IAG
−3.79	37.11	12	289	76	−100	143	17	−56	505	20	030910A	IAG
−2.07	37.36	4	58	29	97	230	61	86	222	20	031030	IAG
−2.71	37.57	9	163	45	−92	346	45	−88	183	22	031116	ETH
−1.38	37.67	4	335	82	−149	240	60	−8	811	20	040416	IAG
−3.32	36.67	18	53	59	−117	278	41	−53	596	21	041106	IGN
−1.78	37.88	10	132	85	−153	40	63	−5	162	22	050129	IAG

Table 1. (continued)

Longitude	Latitude	Depth	S1*	D1**	R1***	S2*	D2**	R2***	Sc	Iexp	Name	Catalog
−1.7	38.02	6	120	68	−125	1	40	−35	261	20	050201	IAG
−1.79	37.82	10	110	84	−136	15	46	−7	244	21	050203	IAG
−1.8	37.82	6	109	82	−136	11	47	−10	865	20	050204	IAG
					Iberian Chain (6)							
−1.48	40.47	10	146	51	−55	279	50	−125	98	24	960803	IAG
−1.69	40.45	20	145	58	−82	313	33	−100	31	21	980725	IAG
−8	38.83	8	49	89	−38	140	51	−178	11	22	010923A	IAG
−2.8	38.95	4	148	76	−96	351	15	−68	112	20	030720B	IAG
0	39.39	9	171	59	−70	316	36	−120	201	22	030916	ETH
1	39.39	8	175	58	−48	296	51	−137	166	20	030916B	IAG
4	39.39	8	352	28	−46	125	70	−110	359	21	030921A	IAG
1	39.41	8	148	64	−85	315	27	−101	492	21	030921B	IAG
					Pyrenees (7)							
0	43.12	12	296	58	−92	121	32	−86	103	22	030121	ETH
−1.52	42.88	9	289	65	−92	112	26	−87	947	22	040918	ETH
−3.2	43.05	4	93	18	−93	276	72	−88	453	20	021211	IAG
−3.6	43.02	4	316	84	−92	157	6	−69	273	22	021212	ETH
−1.53	42.87	6	277	61	−94	105	29	−83	194	22	040930	ETH
6	42.9	10	141	38	−47	273	63	−117	26	22	991004	IAG
−1.7	42.93	6	345	57	−52	111	49	−133	855	21	020516	ETH
−5	42.65	15	91	27	−122	307	67	−75	636	23	800229B	HVR
2.17	42.34	8	291	55	−119	156	44	−54	466	21	040921	IAG
					Northern Algeria (8)							
1.36	36.25	10	247	30	105	50	61	81	507	26	801010A	HVR
1.31	35.72	10	58	43	81	250	47	98	224	25	801010B	HVR
2.07	36.53	15	63	42	69	271	51	108	227	24	801013A	HVR
1.32	36.02	15	270	45	126	44	55	59	759	23	801108B	HVR
1.68	35.87	15	112	61	−179	21	89	−29	1127	23	801205A	HVR
1.38	36.38	15	181	53	29	72	67	139	367	23	810115A	HVR
1.9	36.27	15	210	43	64	64	52	112	269	24	810201F	HVR
1.76	36.08	15	26	67	−18	124	73	−156	739	23	810214D	HVR
1.15	35.73	15	274	70	169	180	80	−20	834	23	821115A	HVR
2.76	36.44	6	261	80	102	29	15	39	58	24	881031	IAG
2.65	36.39	2	10	11	11	269	88	101	35	23	890212	IAG
2.92	36.84	15	91	48	119	231	50	62	965	24	891029E	HVR
2.83	36.26	15	49	18	95	225	72	88	82	23	900209A	HVR
2.88	36.98	14	260	70	108	36	26	49	19	24	960904	IAG
1.17	35.94	10	23	45	56	247	54	120	139	23	970714A	INGV
1.37	36.02	4	68	7	113	225	83	87	58	22	000702	IAG
4.97	36.2	21	8	87	−20	99	70	−177	821	23	000818	ETH
4.84	36.47	24	230	68	86	61	22	101	474	22	001110	ETH
4.9	36.43	18	239	65	91	57	25	88	676	24	001110	ETH
4.73	36.62	4	121	88	−98	16	8	−15	29	23	001110B	IAG
4.76	36.66	21	125	84	−138	29	48	−8	321	23	01116	ETH
2.91	36.13	2	58	16	28	302	82	105	276	22	030101	IAG
3.5	36.92	6	247	71	99	41	21	65	277	22	030521D	IAG
3.82	36.96	21	282	67	93	93	23	82	12	23	030521	ETH
3.93	37.07	15	261	73	91	76	17	86	17	23	030521	ETH
3.58	36.93	15	57	44	71	262	49	107	201	26	030521H	HVR
3.61	36.9	15	65	27	86	250	63	92	176	26	030521A	INGV
3.84	36.91	12	260	74	85	99	16	108	211	22	030522	ETH
3.85	37.14	6	75	10	80	265	81	92	823	21	030522D	IAG
3.89	37.17	12	115	70	−156	17	68	−22	185	23	030522	ETH
3.56	37.07	18	235	68	100	31	24	68	285	22	030522	ETH
3.71	37	12	218	69	88	44	21	96	681	21	030522	ETH
3.64	37.08	9	249	76	93	57	14	78	502	23	030522	ETH
3.44	36.76	12	253	65	92	69	25	87	555	21	030522	ETH
3.63	36.88	12	240	70	98	37	21	68	317	22	030522	ETH
3.46	37.68	15	37	12	66	241	79	95	272	23	030522C	IAG
3.75	36.94	9	218	68	98	17	23	71	274	22	030523	ETH
3.76	36.97	12	220	62	100	20	30	73	732	21	030524	ETH
3.97	37.04	18	261	72	92	76	19	85	204	23	030524	ETH
3.76	37.1	15	237	72	100	27	21	61	501	22	030524	ETH
3.96	37.03	15	263	73	94	70	17	77	47	22	030524	ETH
3.59	36.81	15	75	24	96	248	66	87	409	24	030527A	INGV
3.65	37.06	9	15	69	−39	121	54	−154	44	22	030528	ETH

Table 1. (continued)

Longitude	Latitude	Depth	S1*	D1**	R1***	S2*	D2**	R2***	Sc	Iexp	Name	Catalog
3.27	36.88	6	59	21	66	264	70	99	277	22	030528	IAG
3.36	36.82	6	95	53	−173	0	84	−37	323	22	030529	IAG
4.01	36.97	6	271	80	−92	101	10	−80	252	22	030601	ETH
3.46	36.84	12	261	61	88	85	29	93	145	22	030602	ETH
3.84	37.13	12	265	74	89	89	16	94	145	22	030623	ETH
3.65	37.24	21	265	72	81	111	20	115	16	22	030705	ETH
3.9	36.87	9	292	74	−87	100	16	−101	771	21	030706	ETH
3.53	36.75	15	265	70	97	65	21	72	683	21	030714	ETH
3.42	37.45	18	238	79	93	41	11	74	118	22	031012	IGN
3.43	36.94	6	119	86	−111	19	21	−10	206	22	040110	IAG
3.37	36.87	30	284	83	114	29	25	17	482	22	041205	IGN
9.4	36.02	26	277	40	140	39	66	57	291	24	801207A	HVR
3.6	35.6	15	40	23	70	241	69	98	686	24	940818B	HVR
−1	35.46	4	79	24	145	201	77	70	48	22	981210	IAG
−1.28	35.32	8	59	21	118	209	71	80	38	24	991222	IAG

[a]S1*, D1**, and R1*** are strike, dip, and rake, respectively, of plane 1. S2*, D2**, R2*** are Strike, dip, and rake, respectively, of plane 2. Sc denotes scalar moment; Iexp is exponent for moment tensor (CMT catalog).

and the Atlantic, where moderate to large earthquakes occur with certain frequency. Moment tensor projects at the Euro-Mediterranean scale at Italian INGV [*Pondrelli et al.*, 2002, 2004] and ETH-Zürich [*Braunmiller et al.*, 2002] can include additional moderate earthquakes larger than ~4, since the shorter average event-station paths permit an appropriate correction of propagation effects for the intermediate-period wavefield from available, simplified earth models. The Ibero-Maghrebian moment tensor project at IAG-Granada [*Stich et al.*, 2003, 2006] inverts for earthquakes larger than 3.5 from a dense station network and provides the currently largest moment tensor inventory for the region. Finally, in 2003, IGN-Madrid started operating fully automated near-real-time inversion, based on the 3 closest regional recordings for earthquakes larger than 3.3 [*Rueda and Mezcua*, 2005]. Despite the simplified procedure, these estimates show an overall good correlation with the manually processed solutions from the IAG catalogue.

[12] We merged these catalogues to build a moment tensor inventory for the western Eurasia-Africa limit. From among multiple solutions for the same event, when available, we select the solution with the lowest percentage of non-double-couple (CLVD) components of the moment tensors [*Dziewonski and Woodhouse*, 1983], taking into account also the station coverage involved in the different inversions. Our merged moment tensor list for regional stress field analysis contains 210 events between N44° and N34° latitude and 30°W–5°E longitude. The list is shown in Table 1. As the main objective was to constrain the crustal (and uppermost mantle) stress field, we have only considered earthquakes with a hypocentral depth less than 70 Km. These populations will be analyzed to contrast the previous results obtained from first arrivals' focal mechanisms, and to interpret active tectonics where data density permits a good resolution of regional stress conditions.

4. Methodology of Regionalization

[13] To identify areas with similar stress conditions, we carried out a preliminary analysis of the orientation and a stress-strain shape analysis, applying the methodology suggested by *Capote et al.* [1991] based on the "slip model" of triaxial deformation [*Reches*, 1983; *de Vicente*, 1988]. Assuming that one of the strain (stress) tensor principal axes is actually vertical in the vicinity of the free surface, this method directly provides a measure of the shape of the strain ellipsoid ($K' = e_y/e_z$. e_x, e_y, e_z principal strain axes, x, y, z coordinates defined by the strain tensor principal axes) and also the maximum horizontal shortening direction (Dy), for every individual focal mechanism [*de Vicente*, 1988].

$$K' = \left(\sin^2 D \cos^2 B\right)/\left(1 - \sin^2 D \cos^2 B\right) \quad (1)$$

and $B = (\sin^2 D \cos^2 P)$, being D the nodal plane dip, and P the pitch of the slip vector on this fault plane.

[14] K' parameter shows possible values between $+\infty$ and $-\infty$. It was scaled up by a logarithmic scale into the interval +300 (uniaxial compression) and −300 (uniaxial extension) (0, pure strike-slip) (Figure 3). Subsequently, the Dey and the K' values were interpolated in a 1° mesh, obtaining a regular distribution of the direction of maximum horizontal compression and the strain pattern [*Olaiz et al.*, 2006].

[15] This analysis is able to outline zones of homogeneous strain. Together with the tectonic information and the epicentral distribution, it allows the selection of areas with homogeneous stresses where the stress tensor from the classical inversion methods can be calculated (see below). Moreover, the simple view of the K' values distribution shows the presence of extensional strains on the north and NE of the Iberian Peninsula and compression on the Gulf of Cadiz and north of Algeria (Tell mountains). The areas with shear strain (strike-slip faults) are located between (Figures 3a and 3b). The selected areas (although there has been considered different combinations) are: (1) Terceira Ridge, (2) Gloria Fault, (3) Gulf of Cadiz, (4) Western Iberia, (5) Central-Eastern Betics, Alboran Sea and Rif, (6) Iberian Chain, (7) Pyrenees, and (8) northern Algeria.

[16] However, the data density is not homogeneous, and we have tried not to depend on solutions based on low numbers of data (5 in Gloria Fault area). In any case, the

inversions from northern Algeria (58 data) and Rif-Alboran-Betics (95 data) can be considered very well constrained (Figure 4). Although the number of mechanisms allows a more detailed spatial analysis, the recurrence on the average solutions points out the occurrence of very similar tensors, especially in the Tell Mountains. We will discuss in detail the Betics-Alboran-Rif solutions, where inversion misfit is clearly larger than in the other zones (see later). From the epicentral distribution, a NE-SW belt of high epicenters density turns up from the eastern Betics, through Alboran Sea, up to the Rif, limited by two alignments of low seismic occurrence and an area with a clear step of the Bouguer anomalies [*Andeweg and Cloetingh*, 2001].

5. Methodology of Stress Inversion

[17] In the stress inversion analysis, it is assumed that during the faulting process of the upper crust, a set of invariant geometrical properties emerges whose most obvious expression is the Gutenberg and Richter law [*de Vicente et al.*, 2006]. From this point of view, it is possible to carry out the inversion without taking into account, or to scale, the focal mechanisms according to its magnitude. In the same way, there is not a minimum representative magnitude of the state of the tectonic stresses, so the only applied criterion is that of solution quality.

[18] Since most inversion methods are based on striation-fault pair orientations, it is necessary to choose between the two nodal planes to decide which one to introduce into the inversion (the exception is the Right Dihedral Method [*Angelier and Mechler*, 1977] which is usually used at the beginning of the analysis). We have chosen the same strategy followed in two previous papers, where we first used P arrivals focal mechanisms [*Consejo de Seguridad Nuclear*, 1998; *Herraiz et al.*, 2000], to select the ''new-formed'' plane. This will also allow us to compare the inversion results from these two different ways of calculating focal mechanisms (first p arrivals and moment tensor focal mechanisms).

[19] Thus the quality of the inverted stress solution is much better, and explains more faults, even though the tensor results are very similar, whether we take into account only the reactivated planes or both [*de Vicente*, 1988; *Giner-Robles et al.*, 2006]. The newly formed plane selection can be carried out on the basis of the Andesonian failure criterion, but such a procedure involves strong assumptions and may lead to misinterpretations. Instead, we use the predicted symmetries from the Slip Model of triaxial strain [*Reches*, 1983; *de Vicente*, 1988; *Capote et al.*, 1991]. With this procedure, there is no certainty about which nodal plane was the active fault plane, but it improves notably the quality of the stress tensor solution.

[20] *Wallace* [1951] and *Bott* [1959] established the basic principles of a fault sliding under a given stress field. Furthermore, *Bott* [1959] proposed that the slip in any fault will occur on the highest shear stress direction projected on this plane (Bott equation). The first inversion method for fault populations was proposed by *Carey and Brunier* [1974]. They assumed that the slikenslides coincided with this orientation, although this hypothesis has been discussed for a long time.

[21] In practice, the overall obtained results, especially from focal mechanism populations were highly congruent in many different tectonic settings [*Vasseur et al.*, 1983; *Angelier*, 1984; *Michael*, 1987; *Delvaux*, 1994].

[22] In our case, the Stress Inversion Method was chosen [*Reches et al.*, 1992] owing to the fact that it is one of the most restrictive inversion methods. It constrains the fault planes to overcome the frictional resistance (Coulomb criterion). The solution, for every population, is selected from the different friction values, depending on two criteria of angular quality: the slip (SLIP) misfit and the principal (PPAL) angle misfit (Z. Reches, SoftStructure-Structural Geology on a Personal Computer, programs for quantitative analysis in Structural Geology, 1996, http://earth.es.huji.ac.il/reches/soft.html), and it provides the shape factor ratio,

$$R = (S_2 - S_3)/(S_1 - S_3), \quad (2)$$

the orientation of the main axis of the stress tensor (S_1, S_2, S_3), and the friction coefficient. To check the statistical representative of the focal mechanism sample to obtain the solution, a bootstrapping process, Monte Carlo type, was carried out for the friction value with the smallest errors. This technique allows determination of the possible dispersion on the main axis location, especially potential permutations between two principal axes of the solution tensor, when two of them have similar magnitudes. Finally, the fault planes and the stress tensor solution have been plotted on the Mohr circle. In this way, the new-formation (faults on the circle)/reactivation (faults within the circle) characteristics of the fault population can be characterized. Rose diagrams of explained faults and stereographic projection of the obtained principal axis were also taken into account when tectonic implications are analyzed. The selected populations and the achieved results are shown in Table 2 and on Figure 4.

6. Active Stresses Results

[23] The types of active tectonic stresses that are deduced from the previous analysis are variable in the region and include extension, compression and intermediate shear stresses, sometimes affecting well-defined areas and others in complex, changing scenarios (Table 2) (Figures 4, 5a, and 5b).

[24] Extension stresses are founded on: Terceira Ridge (location 1 in Figure 5) (almost radial extension), Pyrenees (location 7) and Iberian Chain (location 6). In the Iberian Chain, the extension is also close to radial, whereas in the North of Iberia it seems that an extension a little closer to uniaxial predominates. More than 30% of the focal mechanisms of the Betics-Alboran-Rif area (locations 5 and 5E) can only been explained by means of an almost radial extension, without excluding the possibility of subdividing the solution in two orthogonal uniaxial extensions.

[25] Compressional stresses (uniaxial compression) are located: in the north of Algeria (location 8) and in the Gulf

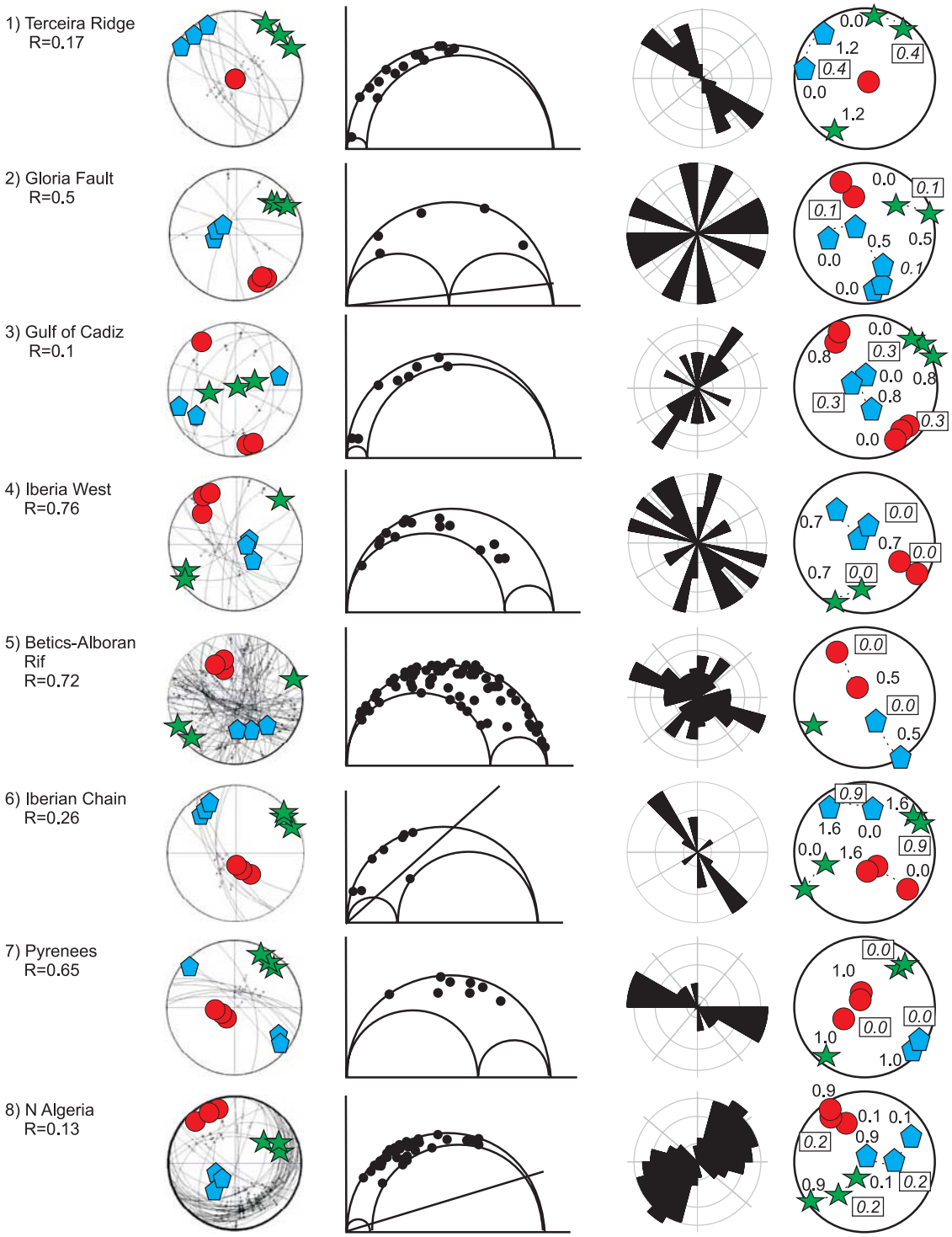

Figure 4. Stress inversion results from the selected zones. From left to right: Stereoplot (lower hemisphere, equal angle) of the inverted nodal planes, and location of principal stress axes at the first and second deviation levels (black circle, S_1, grey pentagon S_2, white arrow S_3); Mohr's circle projection of the selected solution; rose diagrams of the explained nodal planes; and solution set varying the friction coefficient.

Table 2. Selected Populations and the Achieved Results[a]

Regionalization	Zone	N(Nad)	SHmax	R	Slip	Principal	Coefficient	Cohesion	S1	S2	S3	N/R
1	Terceira R	13(14)	137	0.17	5	13	0.4	0.0032	87/154	03/316	01/047	N
2	Gloria F.	5(5)	150	0.5	11	24	0.1	0.0104	15/153	66/281	18/58	R
3	Cadiz G.	9(9)	162	0.1	16	26	0.3	0.0802	02/162	03/252	86/45	N
4*	W Iberia	14(15)	145	0.76	17	27	0.1	0.0197	13/327	74/113	08/235	R
5**	BetAlbor	95(95)	155	0.72	28	30	0.01	0.0338	44/336	46/153	02/245	B
6	IberianCh	7(7)	152	0.26	11	18	0.9	0.0068	69/159	21/328	04/059	N
7***	Pyrenees	9(9)	125	0.65	13	20	0.01	0.0007	68/242	09/131	21/37	R
8	Algeria	51(58)	150	0.13	16	20	0.3	0.0504	10/331	25/66	62/221	N
4	W Iberia	14(15)	145	0.76	17	27	0.1	0.0197	13/327	74/113	08/235	R
4A	Galicia H	8(8)	150	0.58	5	20	0.5	0.0062	84/295	05/151	04/061	A
4B	Galicia S	7(10)	150	0.43	9	24	0.3	0.0670	35/330	55/149	00/240	B
4C	Galicia G	6(12)	123	0.3	20	38	0.9	0.1986	10/303	68/059	20/210	C
5A	Albo_tot	95(95)	155	0.72	28	30	0.01	0.0338	44/336	46/153	02/245	R
5B	Albo-20	48(48)	155	0.73	7	20	0.1	0.0074	46/335	44/155	00/245	
5C	Albo-15	41(41)	154	0.7	7	20	0.1	0.0052	42/333	47/155	01/064	
5D	Albo rev	13(13)	168	0.04	14	21	0.3	0.0625	06/347	68/242	21/80	
5E	Albo+20	30(30)	140	0.29	25	39	0.3	0.0305	88/233	01/345	02/075	
5F	Alhuce	16(16)	155	0.29	10	19	0.1	0.0089	03/335	83/92	07/245	
5G	>depth15	12(14)	149	0.56	13	21	0.1	0.0083	21/326	65/178	12/061	
5H	GranadaB	8(8)	120	0.22	11	28	0.6	0.0088	77/161	09/293	10/024	
7B	PyrRivera	50	125	0.66	0				66/266	20/125	10/032	

[a]S1*, S2*, and S3* are dip and strike of principal stresses. N denotes number of events, and Nad is number of events for the given solution (adjusted). Regionalizations are as follows: 1, Terceira Ridge; 2, Gloria Fault; 3, Gulf of Cadiz; 4, Western Iberia; 5, Central-Eastern Betics, Alboran Sea, and Rif; 6, Iberian Chain; 7, Pyrenees; 8, N Algeria; 4*: 4[a], Galicia subpopulation from 4; 4B, Galician Focal mechanisms from SIGMA Project; 4C, Galician Focal mechanisms from GASPI Project; 5**: 5[a], Albo tot, Central-Eastern Betics, Alboran Sea, and Rif (Total); 5B, Albo-20, slip error < 20°; 5C, Albo-15, slip error < 15°; 5D, Albo rev, only reverse faults; 5E, Albo+20, excluded faults from Albo-20 and Albo rev; 5F, Alhoucemas seismic crisis; 5G, depth > 15 km; 7***, Arudy.

of Cadiz (location 3). Also, the more reverse faults subpopulation from the Betics-Alboran-Rif (location 5) comes closer to uniaxial compression (location 5D), but within the strike-slip regime.

[26] Shear stresses (strike-slip) are founded: in the Gloria Fault area (location 2 in Figure 5) (pure strike-slip), Betics-Alboran-Rif (location 5), closer to uniaxial extension; and in Western Iberia (location 4).

[27] The maximum horizontal shortening directions (S_{hmax}) do not vary more than 25° for all the solutions (except for Pyrenees), with the dominant regional trend having a progressive clockwise rotation from NW-SE to NNW-SSE between the Terceira Ridge and the Gulf of Cadiz. Compressional solutions and reverse subpopulations show a closer to N-S compression (N165°E).

[28] In the Azores Islands (Terceira Ridge), S_{hmax} is parallel to the active fault trends and to the volcanic axis. Increasing the friction coefficient, S_{hmax} approaches a more N-S direction. Faults are new-formed (Figure 4).

[29] In the Gloria Fault zone, activated fault trends are varied and reactivated. Increasing friction produces solutions with S_2 closer to the vertical. The same tendencies are observable in the Gulf of Cadiz, differing only in that faults are newly formed (Figure 4). This contrasts with the notion that reverse faulting earthquakes in the Gulf of Cadiz could involve the reactivation of normal faults that formed during continental breakup [*Gràcia et al.*, 2006; *Zitellini et al.*, 2004].

[30] From these results, it is necessary to indicate the absence of active orogenic compressional tensorial conditions in the Betics-Rif System. This is not the case in the Tell Mountains (north of Algeria), where a NW-SE uniaxial compression is well established. It is perpendicular to the tectonic and topographic trends of the zone, which indicates widespread thrusting of the continental crust of Africa over the Alboran domain and vice versa. These structural trends appear segmented by right lateral strike-slip faults [*Braunmiller and Bernardi*, 2005], also activated by the calculated stress tensor. This results in some kind of strain partitioning that is also visible in the other areas close to the Eurasia-Africa border [*Vázquez and Vegas*, 2000]. All together, the active structures and the epicentral distribution draw a series of "en echelon" thrusts stepped by strike-slip faults, although field observations indicate that the activity of these Neogene-Quaternary structures is not always recent and simultaneous (Figures 2 and 3).

[31] Tensorial and tectonic setting from the Gulf of Cadiz-Gorringe Bank zone is very similar to that of north Algeria, but with a S_{hmax} slightly more toward the NNW and affecting thinned continental crusts of Iberia and Africa. To the west, on oceanic crust, the situation seems to gradually change to pure shear stresses on the Gloria Fault zone (but here only 5 focal mechanisms were available for the inversion). These results, very similar to those obtained by *Stich et al.* [2005a], are quite coherent with the right lateral transpressive character of the Africa-Iberia border up to the Betics-Rif System. This is probably the source area of the Great Lisbon Earthquake of 1755 with an estimated magnitude of 8.5–9, one of the most destructive seisms in European history.

[32] In Western Iberia (Portugal and westernmost Spain), a clear N-S variation on stress conditions appears (Figure 3a).

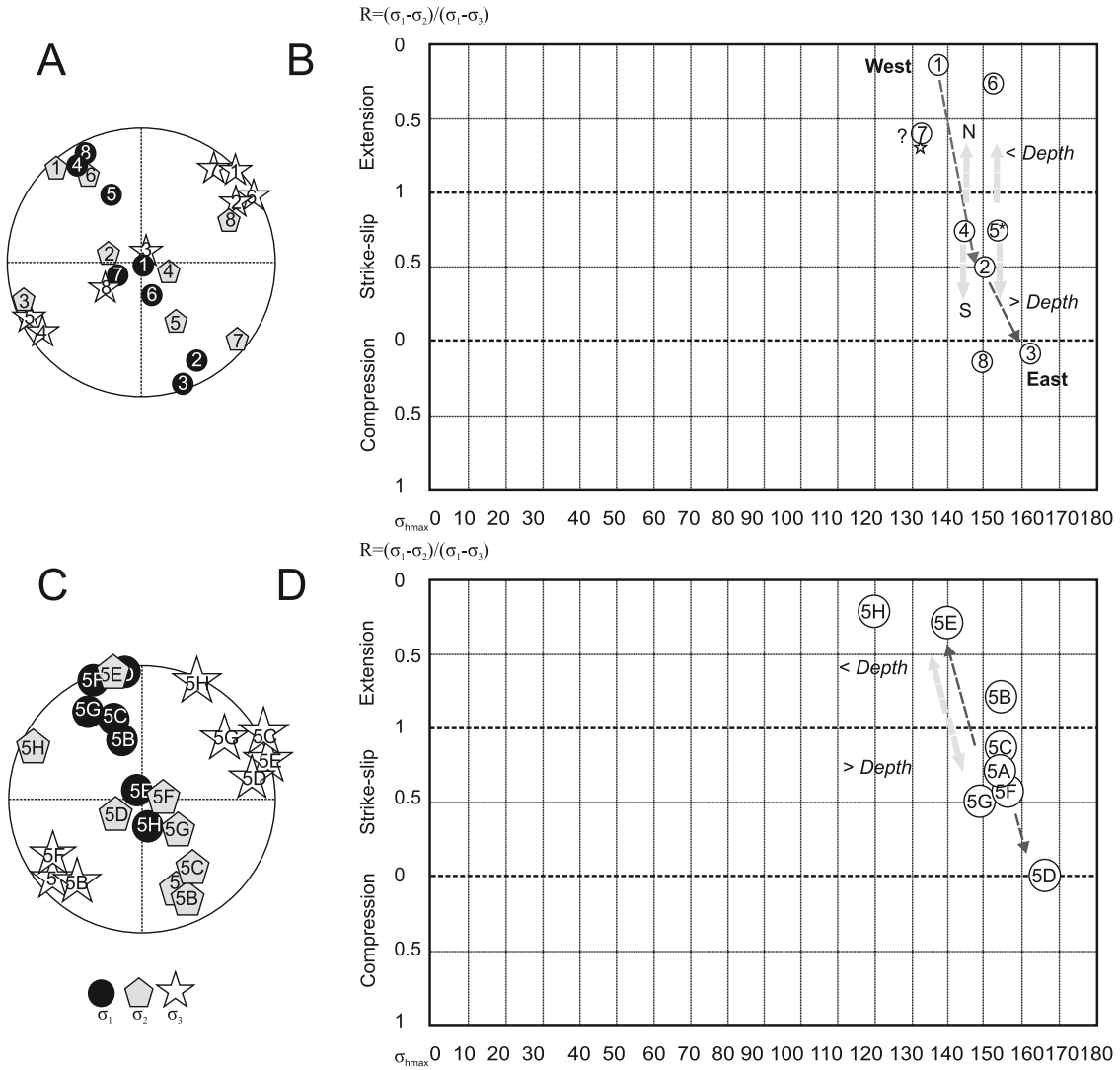

Figure 5. (a) The stereoplot (lower hemisphere, equal angle) of the principal axes of the inverted tensors from every analyzed zone. The corresponding errors and R values are given in Table 2. (b) R/S_{hmax} diagram of the solutions of the selected zones. Note the transition from west to east (dark grey arrow) among 1 (Terceira Ridge), 2 (Gloria Fault), and 3 (Gulf of Cadiz). Within the zones 4 (Western Iberia) and 5 (Central-Eastern Betics, Alboran Sea, and Rif), local tendencies (light grey arrows) are founded from north to south and between deep and swallow earthquakes (see text). (c) The stereoplot (lower hemisphere, equal angle) of the principal axes of the inverted tensors from the Betics-Alboran-Rif zone. The corresponding errors and R values are given in Table 2. (d) R/S_{hmax} diagram of the solutions of the Betics-Alboran-Rif zone. Solutions are as follows: 5A, Central-Eastern Betics, Alboran Sea, and Rif (Total); 5B, slip error < 20°; 5C, slip error < 15°; 5D, reverse faults only; 5E, excluded faults from Albo-20 and Albo rev; 5F, Al-Hoceimas seismic crisis; and 5G, Focal depth > 15 km. Solutions fitted to different errors (solutions 5A, 5B, and 5C) provide similar stress tensor. The most different solutions in the R ratio (solutions 5D-5E) also imply different S_{hmax} (black arrow). Increasing the focal depth results in a strike-slip stress tensor (5G) (light grey arrow). Solution 5H is stress solution for the Granada Basin.

It changes from compression in the south to extension in the north, within average shear stresses conditions. From this perspective, it is logical not to find a well-fitted tensorial solution for the entire zone, as in fact happens. Continental strike-slip faults are mainly activated, as shown by the epicentral alignments and by the rose diagrams of the new-formed active faults (Figures 2 and 4). Increasing the friction coefficient, S_1 approaches vertical and facilitates the interchange between S_1 and S_2.

[33] Seismicity is being nucleated on right lateral strike-slip faults, like the Zufre Fault [*de Vicente et al.*, 2006], mainly southward. In addition, very large left lateral strike-

slip faults are absorbing some part of the deformation. The Regua-Verin-Vilariça-Bragança Fault system especially was active during the Pliocene and the Quaternary [*Cabral*, 1989; *Cabral et al.*, 2004]. Smaller normal and reverse faults can also move under these conditions. Westernmost part of the Central Iberian Ranges (Central System, Figures 1 and 2), mainly on Portuguese territory, they exhibit reverse focal mechanisms, even on larger earthquakes like the 04 23 1909 M_W 6.0 earthquake [*Stich et al.*, 2005b]. Therefore in this zone NW-SE thrusting could have been active during the whole Neogene, related to a similar stress field that has been building up for tens of millions of years and that extends up to the Gulf of Cadiz.

[34] In the Pyrenees, the results indicate a triaxial extension (close to uniaxial extension, R = 0.65) with N35°E trending S_3, perpendicular to the main epicentral alignments (Figure 2) and to the active fault trends (Figure 4), especially in the western most part of the range. Increasing the friction coefficient, S_1 approaches to vertical. Faults are reactivated.

[35] These stresses are very similar to those determined from the aftershocks of the 1980 Arudy earthquake (50 mechanisms, R = 0.66 and S_3 in N32°E) [*Gallart et al.*, 1985; *Rivera and Cisternas*, 1990], but very different from those obtained from first P arrivals focal mechanisms regional analysis [*Goula et al.*, 1999; *Herraiz et al.*, 2000], which taken together imply a strike-slip regime with N10°E S_{hmax}. *Rigo et al.* [1997] found mechanically incompatible solutions and a great variety of focal mechanisms (50), but at least half of the data is compatible with a NE-SW extension.

[36] Nevertheless, WNW-ESE faults with evidence of Quaternary activity, like the Lourdes fault, show clear normal displacements [*Alasset and Megharoui*, 2005]. If this extension is linked in depth to the performance of big thrusts, or to postorogenic isostatic responses, it can be deduced from the surrounding state of stresses: there is no a tensorial stress distribution tied to a clear orogenic environment. Thus the hypothesis of the normal readjustments or postorogenic topographic compensations is the one that turns out to be most reasonable. This would support a geodynamic relevance of recent GPS observations suggesting minor (~0.5 mm/a) moving away between Iberia and Western Europe. Though such small movements are still statistically insignificant at individual stations, a good consistency among GPS velocities over intraplate Iberia backs up the result [*Stich et al.*, 2006].

[37] Inside the Iberian Peninsula, the most extensive situation is located in the Iberian Chain, activating NW-SE normal faults that turn out to be the principal directives of the chain (and of the Mesozoic rift too). They are also visible epicentral alignments of the same orientation (Figure 2). This extension would be superimposed on the one related to the opening of the Valencia Through during the Pliocene, activating NW-SE faults like that of the Jiloca [*Simón-Gómez*, 2004].

[38] In the Betics-Alboran-Rif zone, the inversion is not a single tensor solution, but the superposition of at least 3 mechanically incompatible solutions. The average solution indicates a regime of active stresses of uniaxial extension (R = 0.72) with close to 45° plunges of S_1 and S_2 (Inversion 5A, Table 2). Applying a Monte Carlo procedure, we could show that this peculiar orientation of the stress tensor is due to an interchange between S_1 and S_2 with similar stress magnitudes. In this case, only the S_3 odd axis is significant from a geological point of view. As in Western Iberia, when increasing the friction coefficient, S_1 approaches to vertical and facilitates the interchange between S_1 and S_2. Reactivated and new-formed faults occur (including a majority of the ones just mentioned), with a variety of activated trends, but concentrated in normal NW-SE and right lateral strike-slip faults (Figure 4).

[39] Though the errors are moderate (Table 2), the fittings for lower errors (20° and 15°) give rise to stress tensor solutions that are very similar (R = 0.73, 5B and 0.7, 5C). However, these solutions can only explain half of the focal mechanisms of the population. Again, S_1 and S_2 appear with intermediate plunges. The same tendency is observed after modifying the friction coefficient (in the solution, low frictions favor strike-slip like tensorial solutions) (Figure 4). In this case, the improvement in the solution adjustment reduces the error in the orientation of S_3, but not in S_1 and S_2. This behavior is typical when R is close to 1 or to 0, and then only one axis position can be determined, leaving the two others unconstrained on a perpendicular plane.

[40] The rest of the population (initial slip errors larger than 20°) can be subdivided in turn, between normal and reverse faults. The subpopulation of reverse mechanisms (13 mechanisms, 5D) provides a good investment solution within strike-slip regime close to uniaxial compression that activates thrust and strike-slip faults simultaneously, though the orientation of S_1 comes closer to a N-S trend, as the activated reverse faults have E-W to ENE-WSW directions and are orthogonal to the major kilometer-sized folds that are developed in the region.

[41] The remaining mechanisms (population 5E, Table 2) can only adjust, with not very high errors, to an extension close to radial. Thus they are not able to exclude the concurrence of several uniaxial extensions with different S_3 orientations.

[42] In the Tell Mountains, the solution is very well constrained. Increasing the friction coefficient favors the interchange between S_2 and S_3, and stress conditions close to strike-slip. Almost all the faults are newly formed and perpendicular to S_{hmax} (Figure 4).

[43] In order to compare the different tectonic settings of this region, we will discuss the differences between the present-day crustal stresses near the plate boundary and ones that are located farther away, in intraplate locations.

7. Discussion on Key Zones: The Betics-Alboran-Rif Plate Contact

[44] Moment tensor mechanisms over the Betic-Alboran-Rif area show the largest variability among the populations analyzed, with faulting style ranging from purely normal to purely reverse, suggesting new-formed and reactivated fault activity under different local stresses and stress permutation

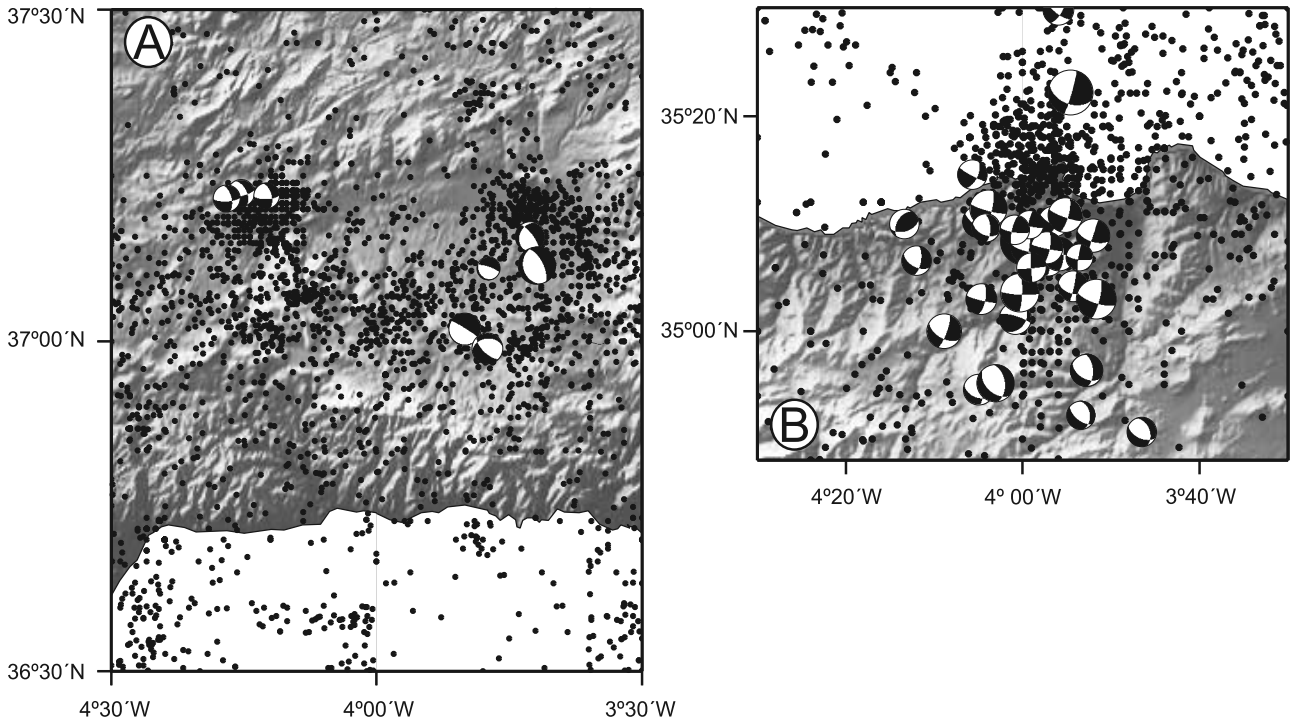

Figure 6. (a) Epicentral distribution and focal mechanisms around the Granada Basin. (b) Focal mechanisms of the Al Hoceima earthquake of 26 May 1994 and its aftershocks in the Rif.

processes. This can be attributed to potential fault interactions and local stress transfer in an area of distributed tectonic deformation [*Stich et al.*, 2006]. Within this heterogeneity, the main appreciable regional trend a tendency toward more significant normal slip components for events located to the NW of the region, compared with strike-slip behavior and occasional reverse slip for events located toward the SE of the earthquake distribution. This tendency is reflected in the regional trend of K′ values. To explore this hypothesis, we have inverted two well constrained subpopulations: Focal mechanisms close to the Granada Basin in the central Betics (Figure 6a) (5H in Figures 5c and 5d), where a clear triaxial and radial extensions are geologically well documented during the Quaternary [*Galindo-Zaldívar et al.*, 1993, 1999], and the 2004 Al Hoceima earthquake sequence in the eastern Rif (Figure 6b) (5F in Figures 5c and 5d). The result from this last population indicates a clear strike-slip regime with the same S_{hmax} orientation as the mean solution (N155°E). On the contrary, Granada Basin inversion shows triaxial extension (R = 0.22) with a N120°E S_{hmin} trend that activates E-W and NW-SE normal faults. Though with this R value, S_2 orientation is not well constrained, the deduced active fault trends are those mapped as Quaternary faults, leading us to think that this S_{hmax} local bend is realistic. Outside the Granada Basin, the Betics focal mechanisms fit also with strike-slip regime close to uniaxial extension, meaning we cannot be sure if it is a N-S gradient of the type of stresses or a local effect related to the development of the highest topography of the Betic Cordillera, related to the a recent crustal extension and the development of large Neogene-Quaternary basins like the Granada Basin.

[45] We have further explored the possibility of stress regime's changing with depth. To extract an appropriate subset of deeper crustal earthquakes, we select a hypocentral cutoff depth such that the deep data set is possibly not too small and is possibly not too contaminated by shallower earthquakes with erroneous depth estimates. For a cutoff depth at 15 km, we can retain 14 mechanisms to analyze deep crustal stresses and expect to avoid a relevant contribution of mislocated, very shallow events, especially those linked to tectonic deformation in the context of Neogene intramountain basin formation. This data set (5G in Figures 5c and 5d) gives rise to a pure strike-slip solution, far from the average uniaxial extension obtained from the entire data set, with a similar S_{hmax} trend (N149°E). If the zone behaves at depth as a strike-slip shear zone, this variety of seismotectonic regimes can be easily explained throughout stress permutations (switches) related to elastic rebound and block accommodation phenomena [*Galindo-Zaldívar et al.*, 1999] and to variations in mechanical coupling across the strike-slip zone that induces changes in extension trends [*Angelier et al.*, 2004]. In our case, reverse focal mechanisms produce a solution with S_{hmax} rotated clockwise from the mean inversion, whereas from normal faults populations S_{hmax} appear to be rotated counterclockwise.

[46] In paleostress and present-day stress analysis from the Granada Basin [*Galindo-Zaldívar et al.*, 1999], the permutations are also frequent between S_1 and S_2, and even S_3, from vertical to horizontal, which has been interpreted

as periodic changes between the performance of extension, strike-slip and even reverse stresses in short time periods [*Reicherter and Peters*, 2005].

[47] These different stress regimes would not indicate, therefore, the performance of successive tectonic stages in the Betics and Rif [*Medina*, 1995; *Galindo-Zaldívar et al.*, 1999], which might simplify the evolutionary scheme proposed for some zones of this plate boundary. It is difficult to correlate the local stress evolution of different sectors and may be the consequence of continuous deformation processes that produce all the observed variety of stresses. In any event, the new results suggest that in areas of relatively thicker continental crust, also related with highest topography, with respect to the surrounding continental crust regions (e.g., central Betic Cordilleras, Alboran Ridge and Western Rif Cordilleras, extension stresses dominate in the upper crust as a result of the gravitational collapse. However, in areas of continental/oceanic crust, like the Tell Mountains, or in regions of low topography (Gulf of Cadiz), compressional stresses predominate.

[48] Our results indicate that this permutation is simultaneous, and as a result establishing tectonic ''phases'' depending on homogeneous tensorial solutions turns out to be, once again, inadequate.

[49] The Betic-Rif mountain belt has been interpreted as a symmetrical collisional orogen, partly collapsed through convective removal of its lithospheric mantle root, or as the result of an active subduction process potentially evolving owing to either slab break-off or slab retreat. It has also been interpreted as an asymmetrical, subduction/collision orogen formed through protracted evolution, fully related to the Alpine-Apenninic mountain building [*Michard et al.*, 2002].

[50] Since normal NW-SE and E-W faults are clearly active during the Pleistocene and Quaternary [*Alfaro et al.*, 2001], simultaneous to the development of large folds [*Galindo-Zaldívar et al.*, 2003], our deduced mean uniaxial extension solution fits with the idea that active thrusting on the Betics ended during the Upper Miocene. There is no evidence of E-W compression, and thus no support for the idea of active escape of the Alboran domain toward the West. The increase of extensive stresses toward the surface, together with ongoing active compressional stresses on the Gulf of Cadiz and The Tell, is a matter that any proposed tectonic model must address.

8. Discussion on Key Zones: (Intraplate) Galicia (NW Iberia)

[51] Recent intraplate seismic activity in Galicia (Figure 7b), culminating in an intensity VII (EMS), MW = 5.2 earthquake on 21 May 1997, has increased the interest of seismic studies on this area [*Rueda and Mezcua*, 2001]. All over, the IGN national seismic network has detected 567 earthquakes (Figure 7a) in and around Galicia between 1979 and 2005. Seismic activity is characterized by an irregular distribution in time, including two major seismic crisis in 1979 (M mb_{Lg}; 4.6) and November to December 1995 (M mb_{Lg}; 4.7) before the May 1997 earthquake sequence with two moderate size main shocks (MW = 5.2 and 4.8 [*Stich et al.*, 2003]). This locally dense sampling permits us to use the Galician case for a description of the current intraplate stress conditions. During the Pyrenean Orogeny (Eocene-Oligocene [*Sibuet et al.*, 2004]), most of the N-S convergence between Iberia and Eurasia was transferred southernward from the Cantabrian Mountains (western Pyrenees) across the intraplate fault corridors of Vilariça, Bragança, Regua, Verin up to the Central System (Pyrenean Domain, Figure 7b). Its direction is subparallel to the Atlantic Ocean border (they were a part of the Lower Cretaceous Rift) and its Tertiary movement is left lateral strike-slip. To the west of the transference zone, the amount of residual convergence is partly accommodated by NW-SE right lateral faults (Puentes de García Rodríguez, Meirama) in the continuation of the ''hanging wall block'' of the southern Cantabrian Thrust. The width of the thrusting structures (pop-ups) diminishes from the eastern zone, due probably to the rheological effect of the thinning of the continental crust toward the Atlantic Ocean. In any case, the thrust trends and the available paleostresses information indicate that the NW corner of Iberia was formed by means of a NW-SE S_{hmax} (Atlantic Domain, Figure 7b). In the zone closer to the Atlantic coast, N-S left lateral strike-slip faults are plentiful (during the Lower Cretaceous they probably moved as normal faults, too). The southern end of this thrust system can be also interpreted as a reorientation of the South Cantabrian Thrust westerly from the Vilariça Fault System. This device explains the landscape change in the transition to Asturias, the Cantabrian front of Galicia, the Atlantic Galician front, Central Galicia and the Portuguese frontier zone.

[52] Previous analyses of earthquake focal mechanisms and Pliocene- Quaternary faults [*Consejo de Seguridad Nuclear*, 1998; *Herraiz et al.*, 2000; *Stich et al.*, 2003] show a great variety in the active types of faults, which turns out to be coherent with a regional active strike-slip stress field. Recently, local networks have been deployed (GASPI) [*López-Fernández et al.*, 2004] that have obtained additional focal mechanisms. We will compare three different groups of data to constrain a realistic state of stresses of the zone: regional moment tensor solutions from the Western Iberia subset (4), located in Galicia (group 4A), solutions from the SIGMA project [*Consejo de Seguridad Nuclear*, 1998] (group 4B), and solutions from the GASPI local network (group 4C) [*López-Fernandez et al.*, 2004]. These final two solutions are focal mechanisms from first P arrivals. Inversion results are shown in Table 2 and Figures 7c and 7d.

[53] As discussed before, Western Iberia shows a progressive change in the type of stresses from compression to the South to more extensive solutions to the North. The stress inversion from Galician focal Mechanisms (solution 4A) has a mean S_1 close to vertical and a R value within triaxial extension. This well-fitted solution explains both the majority of normal mechanisms of the Sarria zone (Figure 8), as well as the less frequent and smaller-magnitude strike-slip mechanisms. Conversely, inversion solutions from SIGMA (4B) and GASPI (4C) data sets have vertical S_2

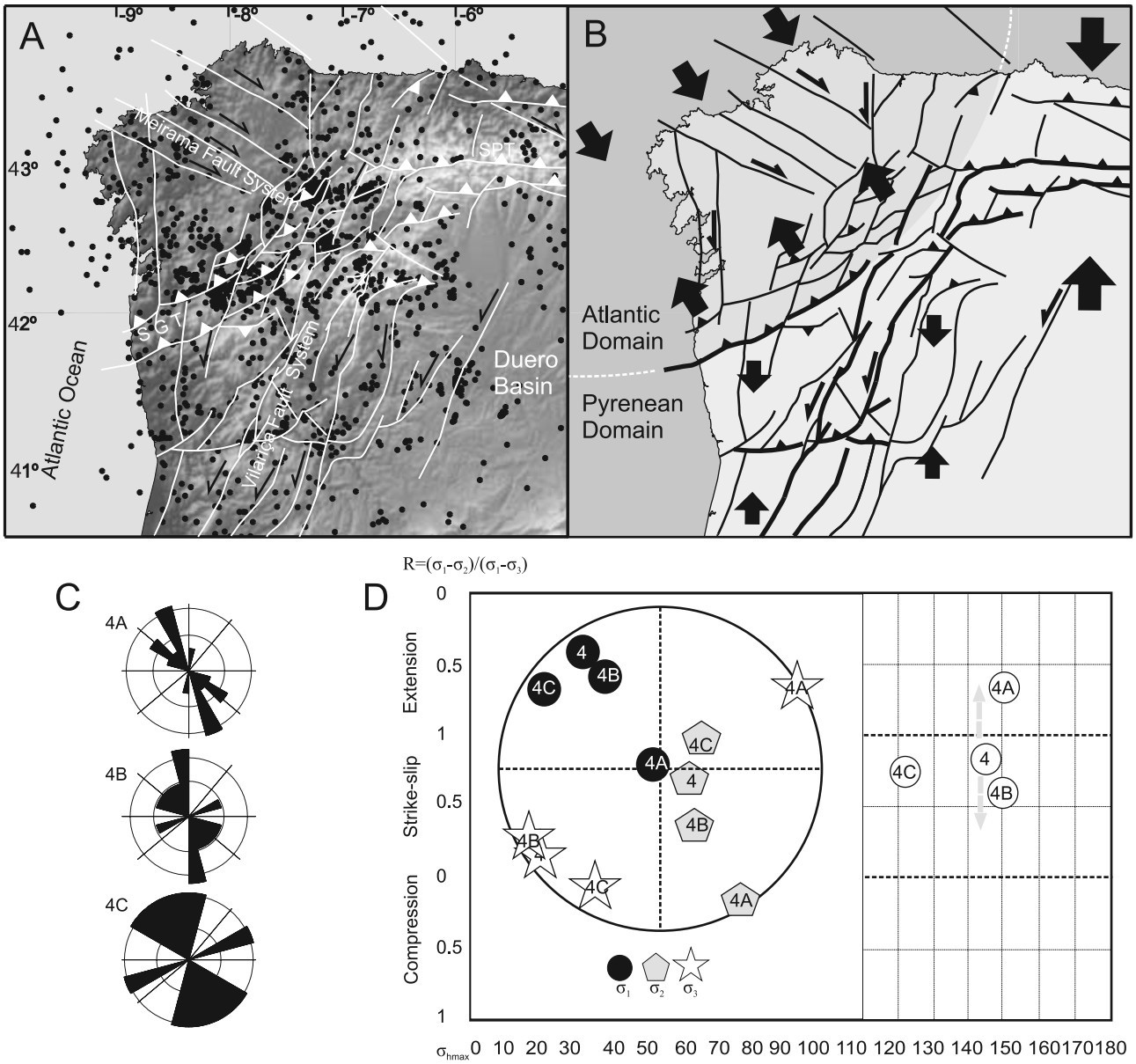

Figure 7. (a) Active faults and paleostress domains of the NW corner of Iberia (Galicia) during the Pyrenean Orogeny (Eocene-Oligocene). (b)Epicentral distribution of the instrumental seismicity (Instituto Geografico Nacional de España online data, 1980–2005, http://www.fomento.es/MFOM/LANG_CASTELLANO/direcciones_generales/instituto_geografico/) from Galicia, and main Cenozoic faults. (c) Rose diagram of the explained nodal planes. (d) R/S_{hmax} diagram of the inverted solutions from Galicia. Solutions are as follows: 4A, Galicia subpopulation from solution 4; 4B, Galician Focal mechanisms from SIGMA project; 4C, Galician Focal mechanisms from GASPI project. Stereoplot (lower hemisphere, equal angle) shows the principal axes of the inverted tensors from Galicia. Corresponding errors and R values are given in Table 2.

pointing out the strike-slip character of the mean result. Solution 4C is the best available from all the GASPI data but explains only half (6) of the focal mechanisms (12). From these last two results, NE- SW reverse focal mechanisms are also explained. As a conclusion, Galician active stress tensor has a NW-SE S_{hmax}. R solutions fall close to uniaxial extension (R = 1). While under this regime NW-SE normal faults are favored, so are NNE-SSW (left lateral) and ESE-WNW (right lateral) strike-slip faults, and subsidiary NE-SW reverse faults can be activated (Figure 7).

[54] Subject to possible location errors for events predating the deployment of local stations, we observe a plausible

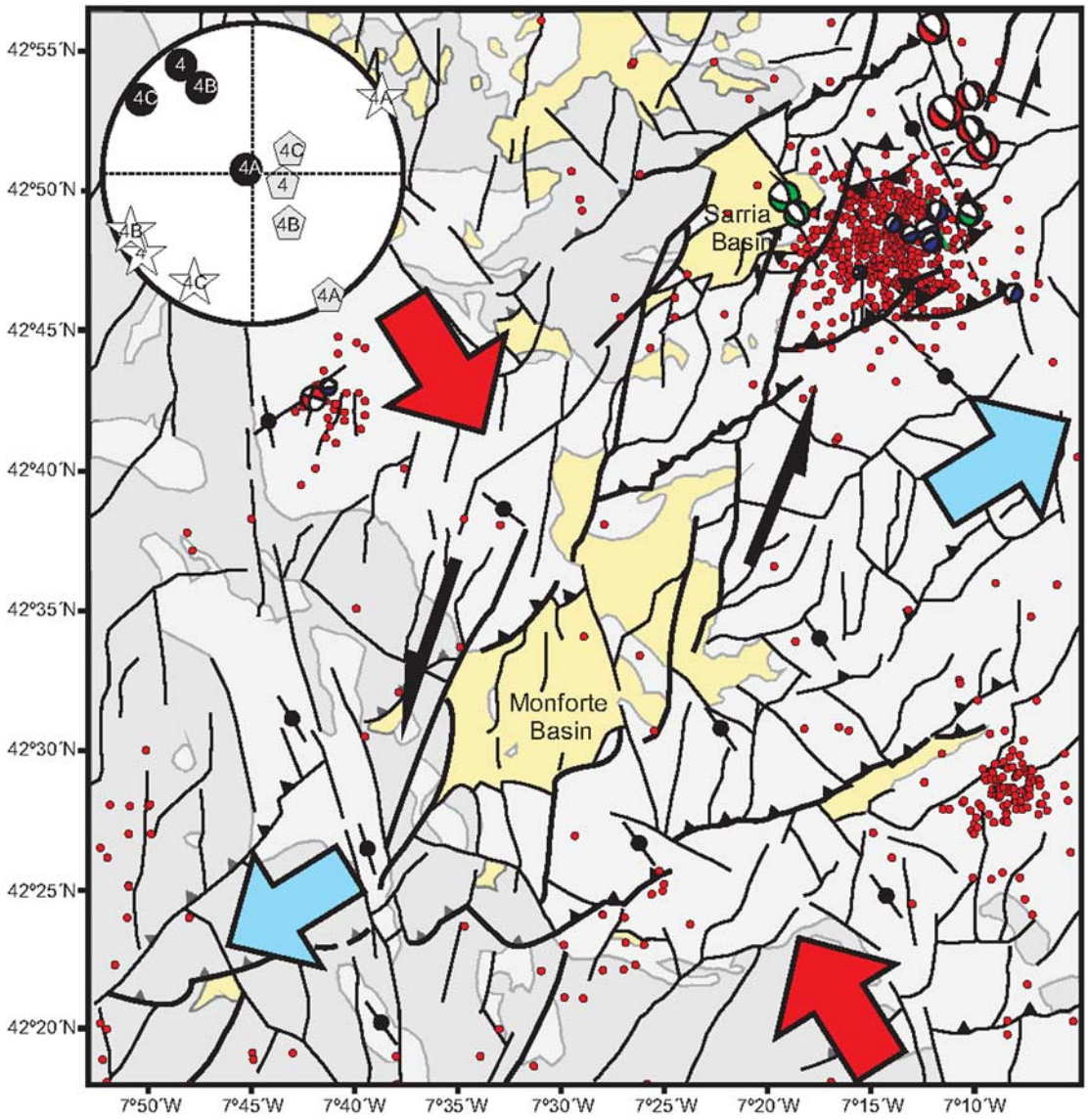

Figure 8. Tectonic map and epicentral distribution of the Sarria and Monforte Cenozoic Basins on restraining bends of the Vilariça Fault System. Principal horizontal axes area also has been drawn.

relation between the epicentral distribution during the Sarria seismic crisis, and local tectonic elements (Figure 8). The main seismic nest is located on a restraining bend of a N20°E left lateral strike-slip fault, belonging to the Vilariça Fault System. Cenozoic basins of Sarria and Monforte were originated through a similar mechanism: They are footwall basins down a left lateral restraining bend of the Vilariça Fault System. Epicentral alignments are consistent with the activation of NW-SE, NNE-SSW and NE-SW faults. The NE-SW fault corresponds to the southern thrust of the restraining bend for what, or it was activated, or it represented a limit to the propagation of the NW-SE alignments occurred in a northwestern direction. Consistently, geological field data point to the occurrence of Quaternary active thrusting [*Rodríguez-García et al.*, 2006].

[55] Therefore, when considering a NW-SE maximum horizontal compression trend, it seems that all compatible fault types have been activated during recent Galician seismicity. This situation is better explained in a general strike-slip stress regime than by uniaxial extension. With these results, it appears that the global solution for Western Iberia (4) can also be applied to Galicia (Strike-slip close to uniaxial extension). In any case, the most important lesson from Galicia intraplate seismicity is probably that, in Western Iberia, seismicity is related to faults that were active during the Cenozoic with similar kinematics.

9. Conclusions

[56] 1. Stress inversions from populations of moment tensor focal mechanisms around Iberia provide better solu-

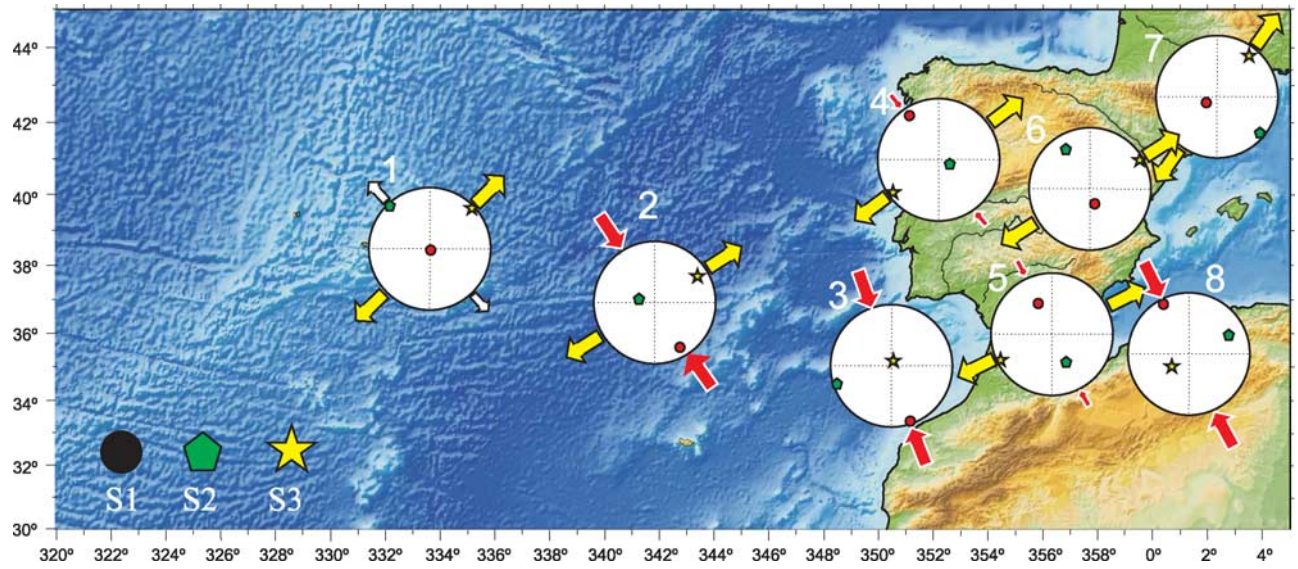

Figure 9. Digital elevation and bathymetry model of the Western Africa–Eurasia limit, with stereoplots (lower hemisphere, equal angle) of the principal axes of the inverted tensors from the different analyzed zones: 1, Terceira Ridge; 2, Gloria Fault; 3, Gulf of Cadiz; 4, Western Iberia; 5, Central-Eastern Betics, Alboran Sea, and Rif; 6, Iberian Chain; 7, Pyrenees; and 8, northern Algeria. Black arrows denote compression. White arrows denote extension. The size is scaled according to the R obtained values.

tion quality than those obtained from the first P arrival polarities. This reflects the generally higher reliability of moment tensor inversion techniques for source parameter retrieval. The use of full waveform information can mitigate intrinsic ambiguities in source estimates from regional networks and consequently reduces the number of gross outliers among the focal mechanism population, which, in turn, would introduce spurious mechanical incompatibilities into the stress inversion. General slip misfits, for selected regional populations of 5 to 95 focal mechanisms, are lower

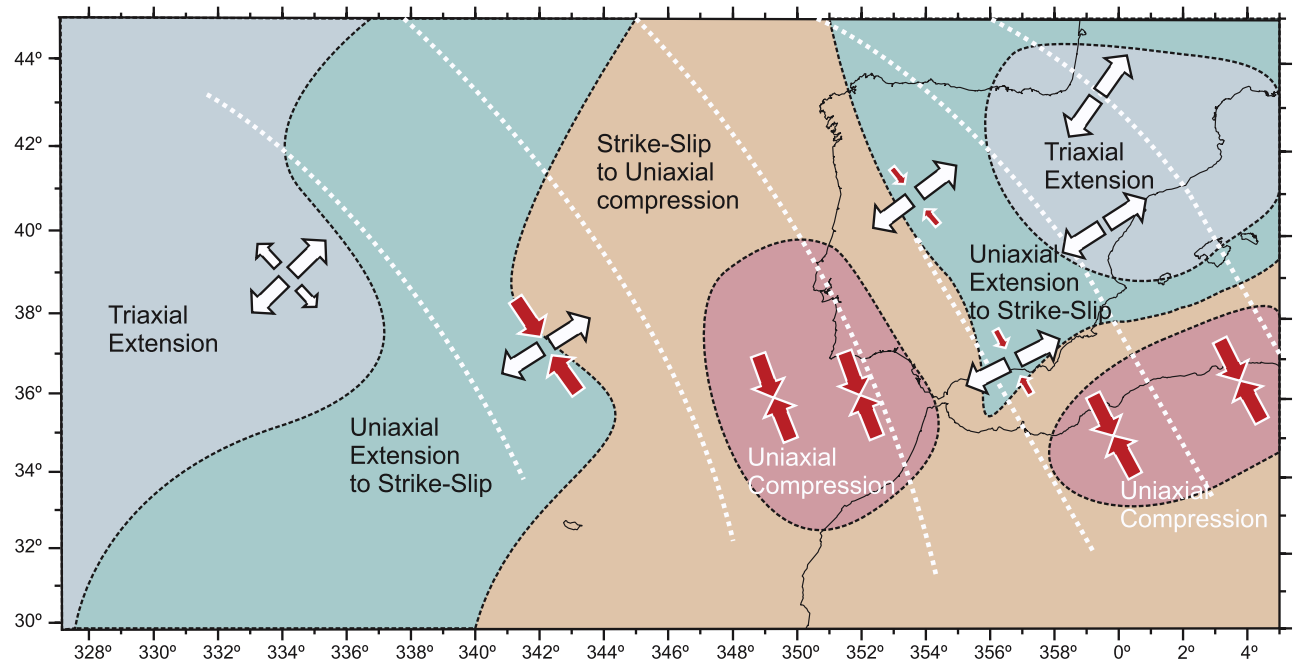

Figure 10. Interpretation of the type of active tectonic stresses of the Western Africa–Eurasia limit. Black arrows denote compression. White arrows denote extension. The size is scaled according to the R obtained values. White lines are extrapolation of the S_{hmax} trajectories.

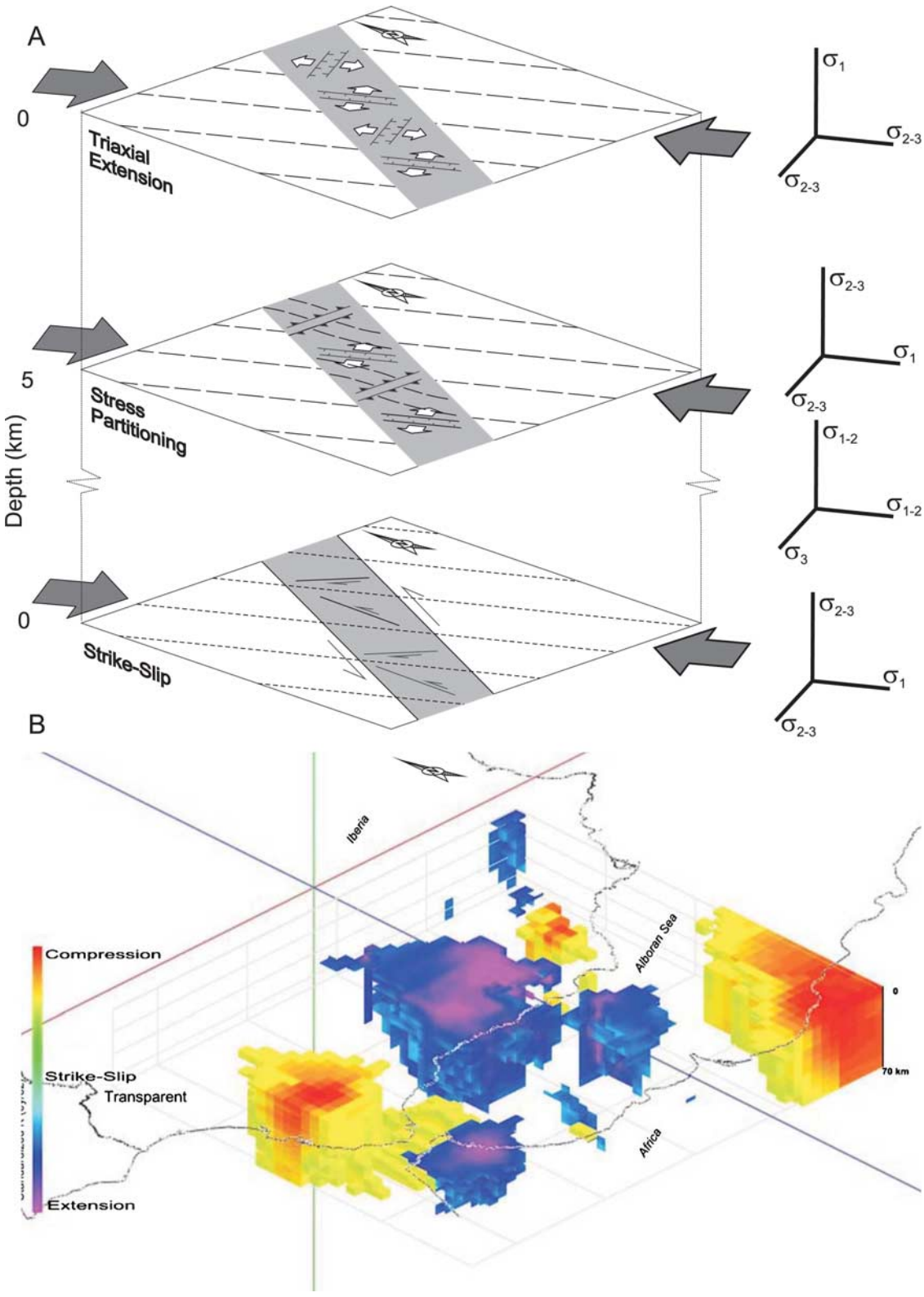

Figure 11. (a) Deduced tectonic active stresses distribution at surface and 15 and 70 km depth in the Betics-Alboran-Rif zone. (b) Parameterized K′ values at different depths (3-D) from the Betics-Alboran-Rif zone.

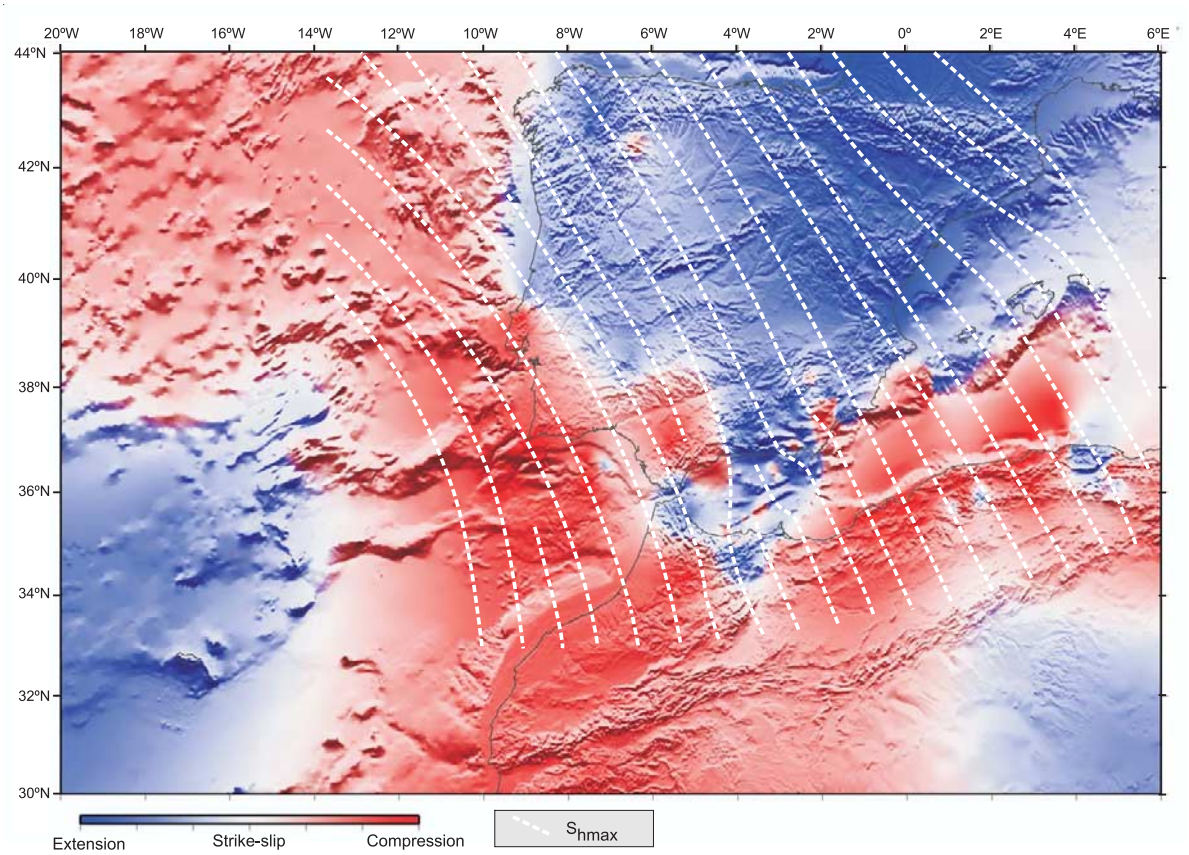

Figure 12. S_{hmax} trajectories of active tectonic stresses around Iberia and parameterized K′ values (see Figure 3a) (blue denotes extension, white denotes strike-slip, and red denotes compression).

than 17° (except 28° for the Betics-Alboran-Rif area, owing to the interference of mechanically incompatible solutions, where selected subpopulations appear with errors lower than 14°).

[57] 2. Along the Eurasia-Africa western boundary, the type of active stresses progressively changes in the east from triaxial extension to uniaxial compression along the Terceira Ridge, The Gloria Fault zone and the Gulf of Cadiz. This is accompanied by a clockwise rotation of the S_{hmax} trend, from N137°E up to N162°E. Both tendencies break down in the Betics-Alboran-Rif zone, where uniaxial extension predominates with a N155°E S_{hmax} (Figures 9 and 10). In the Tell (northern Algeria), uniaxial compression reappears (N150°E S_{hmax}).

[58] 3. In the Iberia foreland zones the extension increases from south to north and from west to east, so in the NE corner of the Iberian Peninsula, triaxial extension appears, whereas the SW zone is close to uniaxial compression. The westernmost part of the Central Iberian Ranges (Montejunto and Sintra in Portugal) undergoes active NE-SW thrusting. Since during the Pliocene, in the eastern part of Iberia, the Central Ranges with similar trends were also active (Guadalupe), it seems to be clear that by maintaining a NW-SE S_{hmax}, extension has migrated westward from the Pliocene up until now. This process must have been simultaneous to the Betics extensional collapse, which avoided the transmission of compressional stresses toward the foreland. Thus the "neotectonic period" (the time span during which the same current stresses have been active) throughout the Iberia foreland, is increasing in length toward the west. Close to the Atlantic border, same tectonic stresses have been acting for tens of million years.

[59] 4. The type of stresses in the Pyrenees, and also the type of neotectonics, is not yet well determined. Unlike the focal mechanisms of the first P arrivals, all (in fact, only 9) seismic moment tensor estimates represent normal faulting. No triaxial extension or strike-slip regimes are able to move the large Pyrenean thrusts. If the extensional situation, consistent with weak evidence from available GPS observations, is confirmed, a N120°E S_{hmax} could be the result of a NW-SE far field stresses plus the topographic effect of the main E-W structural trend of the range.

[60] 5. Undoubtedly, the most complex tectonic situation appears in the Betics-Rif-Alboran zone. In a NE-SW direction, where seismicity concentrates (Figure 2), extension seems to increase toward the N and toward the surface (Figures 11a and 11b). At depth, strike-slip conditions and seismicity distribution uphold the idea of a left lateral shear zone connecting the Gulf of Cadiz and Tell seismic zones undergoing uniaxial NNW-SSE compression. Nevertheless, especially in the Betics, uniaxial extension is the most realistic tensorial situation, the existence of any kind of

triaxial compression can be discarded, as previously was deduced from first P arrival focal mechanisms populations.

[61] 6. Stress trajectories analysis is very well constrained along the plate borders, where data density is high. This is also starting to be the situation in the Iberia foreland zone. Nevertheless, there is a considerable lack of information on the oceanic crust between Portugal and Azores Islands. The clockwise rotation of S_{hmax} among Terceira Ridge, Gloria Fault and the Gulf of Cadiz, together with a NW-SE constant S_{hmax} among the Tell, the Iberian Chain and western Iberia imposes a fan trajectory over the Betics, which is consistent with the presence of extensive stresses in this area (Figure 12).

[62] **Acknowledgments.** This work was mainly funded by the PRIOR project (UCM-CSN-ENRESA-IGN). The study was supported by Consolider Ingenio 2006 "Topo Iberia" CSD2006-00041 and Spanish National Research Program CGL2006-13926-C02-01-02 "Topo Iberia Foreland." These projects are a part of the Spanish contribution to the European Eurocores, TOPO-EUROPE. The authors would like to express their gratitude for the helpful comments of two anonymous reviewers.

References

Alasset, P. J., and M. Megharoui (2005), Active faulting in the western Pyrénées (France): Paleoseismic evidence for late Holocene ruptures, *Tectonophysics*, *409*(1–4), 39–54.

Alfaro, P., J. Galindo-Zaldívar, A. Jabaloy, A. C. López-Garrido, and C. Sanz de Galdeano (2001), Evidence for the activity and paleoseismicity of the Padul fault (Betic Cordillera, southern Spain), *Acta Geol. Hisp.*, *36*(3–4), 283–295.

Andeweg, B. (2002), Cenozoic tectonic evolution of the Iberian Peninsula: Causes and effects of changing stress fields, Ph.D. thesis, 178 pp., Vrije Univ. Amsterdam, Amsterdam.

Andeweg, B., and S. Cloetingh (2001), Evidence for an active sinistral shear zone in the western Alboran region, *Terra Nova*, *13*, 44–50.

Angelier, J. (1984), Tectonic analysis of fault slip data sets, *J. Geophys. Res.*, *89*, 5835–5848.

Angelier, J., and P. Mechler (1977), Sur une méthode graphique de recherche des contraintes principales egalement utilisable en tectonique et en seismologie: La methode des diedres droites, *Bull. Soc. Geol. Fr.*, *7*(19), 1309–1318.

Angelier, J., F. Bergerat, M. Bellou, and C. Homberg (2004), Co-seismic strike-slip fault displacement determined from push-up structures: Selsund Fault, South Iceland, *J. Struct. Geol.*, *26*, 709–724.

Bott, M. H. P. (1959), The mechanism of oblique-slip faulting, *Geol. Mag.*, *96*, 109–117.

Braunmiller, J., and F. Bernardi (2005), The 2003 Boumerdes, Algeria earthquake: Regional moment tensor analysis, *Geophys. Res. Lett.*, *32*, L06305, doi:10.1029/2004GL022038.

Braunmiller, J., U. Kradolfer, M. Baer, and D. Giardini (2002), Regional moment- tensor inversion in the European-Mediterranean area, *Tectonophysics*, *356*, 5–22.

Buforn, E., A. Udías, and M. A. Colombas (1988), Seismicity, source mechanisms and tectonics of the Azores-Gibraltar plate boundary, *Tectonophysics.*, *152*, 89–118.

Buforn, E., A. Udías, and J. Mezcua (1990), Sismicidad y sismotectónica de la región Ibero-Magrebi, *Rev. Geofis.*, *46*, 171–180.

Buforn, E., B. Benito, C. Sanz de Galdeano, C. del Fresno, D. Muñoz, and I. Rodríguez (2005), Study of the damaging earthquakes of 1911, 1999, and 2002 in the Murcia, southeastern Spain, region: Seismotectonic and seismic-risk implications, *Bull. Seismol. Soc. Am.*, *95*, 549–567.

Cabral, J. (1989), An example of intraplate neotectonic activity, Vilarica Basin, northeast Portugal, *Tectonics*, *8*, 285–303.

Cabral, J., P. Ribeiro, P. Figeiredo, N. Pimentel, and A. Martins (2004), The Azambuha Fault: An active structure located in an intraplate basin with significant seismicity (Lower Tagus Valley, Portugal), *J. Seismol.*, *8*, 347–362.

Calais, E., C. DeMets, and J. M. Nocquet (2003), Evidence for a post-3.16-Ma change in Nubia–Eurasia–North America plate motions?, *Earth Planet. Sci. Lett.*, *216*, 8–92.

Capote, R., G. de Vicente, and J. M. González-Casado (1991), An application of the slip model of brittle deformation to focal mechanism analysis in three different plate tectonics situations, *Tectonophysics*, *191*, 399–409.

Carey, E., and M. B. Brunier (1974), Analyse theorique et numerique d'un modele mecanique elementaire applique a l'etude d'une population de failles, *C. R. Acad. Sci.*, *279*, 891–894.

Consejo de Seguridad Nuclear (1998), Proyecto SIGMA: Análisis del estado de esfuerzos tectónicos reciente y actual en la Península Ibérica, *Colección Otros Doc. 10.1998*, 239 pp., Madrid.

Delvaux, D. (1994), Tensor interactive MS-DOS QuickBasic program developed for paleostress determinations on geological fractures and earthquake focal mechanisms, report, R. Mus. for Central Africa, Tervuren, Belgium.

DeMets, C., R. G. Gordon, D. F. Argus, and S. Stein (1990), Current plate motion, *Geophys. J. Int.*, *101*, 425–478.

de Vicente, G. (1988), Análisis poblacional de fallas. El sector de enlace Sistema Central- Cordillera Ibérica, Ph.D. thesis, 317 pp., Univ. Complutense de Madrid, Madrid.

de Vicente, G. (Ed.) (2004), Estructura alpina del Antepaís Ibérico, in *Geología de España*, edited by J. A. Vera, pp. 587–634, Geol. de Esp. (SGE-IGME), Madrid.

de Vicente, G., J. L. Giner, A. Muñoz-Martín, J. M. González-Casado, and R. Lindo (1996), Determination of present-day stress tensor and neotectonic interval in the Spanish Central System and Madrid Basin, central Spain, *Tectonophysics*, *266*, 405–424.

de Vicente, G., S. Martín-Velázquez, M. A. Rodríguez-Pascua, A. Muñoz-Martín, M. Arcilla, and B. Andeweg (2000), Características de los tensores de esfuerzos activos entre la Dorsal Centroatlántica y la Península Ibérica, *Geotemas*, *1*(1), 95–98.

de Vicente, G., A. Olaiz, A. Muñoz-Martín, R. Vegas, S. Cloetingh, J. Galindo, J. Rueda, and J. Álvarez (2006), Campo de esfuerzos activo entre Iberia y Argelia. Inversión de mecanismos focales del tensor del momento sísmico, paper presented at 5th Asamblea Hispano Portuguesa de Geodesia y Geofísica, Com. Española de Geod. y Geofís., Seville, Spain.

Dewey, J. F., M. L. Helman, E. Turco, D. H. W. Hutton, and S. D. Knott (1989), Kinematics of the western Mediterranean, *Geol. Soc. Spec. Publ.*, *45*, 265–283.

Dreger, D., and D. V. Helmberger (1993), Determination of source parameters at regional distances with three-component sparse network data, *J. Geophys. Res.*, *98*, 8107–8125.

Dziewonski, A. M., and J. H. Woodhouse (1983), An experiment in the systematic study of global seismicity: Centroid moment-tensor solutions for 201 moderate and large earthquakes of 1981, *J. Geophys. Res.*, *88*, 3247–3271.

Engelder, T. (1993), *Stress Regimes in the Lithosphere*, 457 pp., Princeton Univ. Press, Princeton, N. J.

Galindo-Zaldívar, J., F. González-Lodeiro, and A. Jabaloy (1993), Stress and palaeostress in the Betic-Rif cordilleras (Miocene to the present), *Tectonophysics*, *227*, 105–126.

Galindo-Zaldívar, J., A. Jabaloy, I. Serrano, J. Morales, F. González-Lodeiro, and F. Torcal (1999), Recent and present-day stresses in the Granada Basin (Betic Cordilleras): example of a late Miocene–present-day extensional basin in a convergent plate boundary, *Tectonics*, *18*, 686–702.

Galindo-Zaldívar, J., A. J. Gil, M. J. Borque, F. González Lodeiro, A. Jabaloy, C. Marín Lechado, P. Ruano, and C. Sanz de Galdeano (2003), Active faulting in the internal zones of the central Betic Cordilleras (SE, Spain), *J. Geodyn.*, *36*, 239–250.

Gallart, J., M. Daignières, J. Gagnepain-Beyneix, and A. Hirn (1985), Relationship between deep structure and seismicity in the western Pyrenees, *Ann. Geophys.*, *3*(2), 239–248.

Giner-Robles, J. L., P. Gumiel, R. Pérez-López, M. A. Rodríguez-Pascua, J. García-Mayordomo, C. Paredes, and J. M. González-Casado (2006), Importancia en la elección de la orientación del plano de falla en el análisis de mecanismos focales de terremotos, paper presented at 5th Asamblea Hispano Portuguesa de Geodesia y Geofísica, Com. Española de Geod. y Geofís., Seville, Spain.

Gölke, M., and D. Coblentz (1996), Origins of the European regional stress field, *Tectonophysics*, *266*, 11–24.

Goula, X., C. Olivera, J. Fleta, B. Grellet, R. Lindo, L. A. Rivera, A. Cisternas, and D. Carbon (1999), Present and Recent stress regime in the eastern part of the Pyrenees, *Tectonophysics.*, *308*, 487–502.

Gràcia, E., et al. (2006), Active faulting offshore SE Spain (Alboran Sea): Implications for earthquake hazard assessment in the Southern Iberian Margin, *Earth Planet Sci. Lett.*, *241*, 734–749.

Grimison, N. L., and W.-P. Chen (1986), Earthquakes in the Davie Ridge–Madagascar region and the southern termination of the African-Somalian plate boundary, *Eos Trans. AGU*, *67*(44), Fall Meet. Suppl., 1105.

Grünthal, G., and D. Stromeyer (1992), The Recent crustal stress field in central Europe, trajectories and finite element modelling, *J. Geophys. Res.*, *97*, 11,805–11,820.

Herraiz, M., et al. (2000), The Recent (upper Miocene to Quaternary) and present tectonic stress distributions in the Iberian Peninsula, *Tectonics*, *19*, 762–786.

Jabaloy, A., J. Galindo-Zaldívar, and F. González-Lodeiro (2002), Palaeostress evolution of the Iberian Peninsula (Late Carboniferous to present-day), *Tectonophysics*, *357*, 159–186.

Jurado, M. J., and B. Müller (1997), Contemporary tectonic stress in northeastern Iberia, new results from borehole breakout analysis, *Tectonophysics.*, *282*, 99–115.

Kiratzi, A. A., and C. B. Papazachos (1995), Active crustal deformation from the Azores triple junction to the Middle East, *Tectonophysics*, *243*, 1–24.

López-Fernández, C., J. A. Pulgar, J. M. Glez-Cortina, J. Gallart, J. Díaz, and M. Ruíz (2004), Actividad Sísmica en el NO de la Península Ibérica observada por la red sísmica local del Proyecto GASPI, *Trabajos Geol.*, *24*, 304 pp.

Mancilla, F., C. J. Ammon, R. B. Herrmann, and J. Morales (2002), Faulting parameters of the 1999 Mula earthquake, southeastern Spain, *Tectonophysics*, *354*, 139–155.

Mazzoli, S., and M. Helman (1994), Neogene patterns of relative plate motions for Africa-Europe: Some implications for recent central Mediterranean tectonics, *Geol. Rundsch.*, *83*, 464–468.

McClusky, S., R. Reilinger, S. Mahmoud, D. Ben Sari, and A. Tealeb (2003), GPS constraints on Africa (Nubia) and Arabia plate motions, *Geophys. J. Int.*, *155*, 126–138.

Medina, F. (1995), Syn- and postrift evolution of the El Jadida–Agadir Basin (Morocco): Constraints for the rifting model of the central Atlantic, *Can. J. Earth Sci.*, *32*, 1273–1291.

Michael, A. J. (1987), Use of focal mechanism to determine stress: A control study, *J. Geophys. Res.*, *92*, 357–368.

Michard, A., A. Chalouan, H. Feinberg, B. Goffé, and R. Montigny (2002), How does the Alpine belt end between Spain and Morocco?, *Bull. Soc. Geol. Fr.*, *173*, 3–15.

Morales, J., I. Serrano, A. Jabaloy, J. Galindo-Zaldivar, D. Zhao, F. Torcal, F. Vidal, and F. Gonzalez-Lodeiro (1999), Active continental subduction beneath the Betic Cordillera and Alboran Sea, *Geology*, *27*, 735–738.

Müller, B., M. L. Zoback, K. Fuchs, L. G. Mastin, S. Gregersen, N. Pavoni, O. Stephansson, and C. Ljunggren (1992), Regional patterns of tectonic stress in Europe, *J. Geophys. Res.*, *97*, 11,783–11,803.

Olaiz, A., G. de Vicente, A. Muñoz-Martín, and R. Vegas (2006), Mapa de esfuerzos de Europa a partir de Mecanismos Focales calculados desde el Tensor Momento Sísmico, *Geogaceta*, *40*, 55–58.

Pondrelli, S., A. Morelli, G. Ekström, S. Mazza, E. Boschi, and M. Dziewonski (2002), European-Mediterranean regional centroid-moment tensors: 1997–2000, *Phys. Earth Planet. Inter.*, *130*, 71–101.

Pondrelli, S., A. Morelli, and G. Ekström (2004), European-Mediterranean Regional Centroid Moment Tensor Catalog: Solutions for years 2001 and 2002, *Phys. Earth Planet. Inter.*, *145*, 127–147.

Randall, G. E., C. J. Ammon, and T. J. Owens (1995), Moment tensor estimation using regional seismograms from a Tibetan Plateau portable network deployment, *Geophys. Res. Lett.*, *22*, 1665–1668.

Rebaï, S., H. Philip, and A. Taboada (1992), Modern tectonic stress field in the Mediterranean region, evidence for variation in stress directions at different scales, *Geophys. J. Int.*, *110*, 106–140.

Reches, Z. (1983), Faulting of rocks in three-dimensional strain fields. II. Theoretical analysis, *Tectonophysics*, *47*, 109–129.

Reches, Z., G. Baer, and Y. Hatzor (1992), Constraints on the strength of the Upper Crust from stress inversion of fault slip data, *J. Geophys. Res.*, *97*, 12,481–12,493.

Reicherter, K., and G. Peters (2005), Neotectonic evolution of the Central Betic Cordilleras (southern Spain), *Tectonophysics*, *405*, 191–212.

Ribeiro, A., J. Cabral, R. Baptista, and L. Matias (1996), Stress pattern in Portugal mainland and the adjacent Atlantic region, West Iberia, *Tectonics*, *15*, 641–659.

Rigo, A., H. Pauchet, A. Souriau, A. Gresillaud, M. Nicolas, C. Olivera, and S. Figueras (1997), The February 1996 earthquake sequence in the eastern Pyrenees: First results, *J. Seismol.*, *1*, 3–14.

Rivera, L. A., and A. Cisternas (1990), Stress tensor and fault plane solutions for a population of earthquakes, *Bull. Seismol. Soc. Am.*, *80*, 600–614.

Rodríguez-García, A., L. Quintana, L. González-Menéndez, and A. Suárez-Rodríguez (2006), Geotectónica en el norte de Galicia: Fallas inversas de actividad cuatrenaria en la cuenca fluvial del alveolo de Alfoz, Lugo, *Geogaceta*, *40*, 23–26.

Roest, W. R., and S. P. Srivastava (1991), Kinematics of the plate boundaries between Eurasia, Iberia, and Africa in the North Atlantic from the Late Cretaceous to the present, *Geology*, *19*, 613–616.

Rueda, J., and J. Mezcua (2001), Sismicidad, Sismotectónica y Peligrosidad Sísmica en Galicia, *Publ. Tech. IGN 35*, 64 pp., Inst. Geogr. Nac., Madrid.

Rueda, J., and J. Mezcua (2005), Near-real-time seismic moment-tensor determination in Spain, *Seismol. Res. Lett.*, *76*(4), 455–465.

Sartori, R., L. Torelli, N. Zitellini, D. Peis, and E. Lodolo (1994), Eastern segment of the Azores–Gibraltar line (central-eastern Atlantic): An oceanic plate boundary with diffuse compressional deformation, *Geology*, *22*, 555–558.

Savostin, L. A., J. C. Sibuet, L. P. Zonenshain, X. Le Pichon, and M. J. Roulet (1986), Kinematic evolution of the Tethys belt from the Atlantic Ocean to the Pamirs since the Triassic, *Tectonophysics*, *123*, 1–35.

Schindler, A., M. J. Jurado, and B. Mueller (1998), Stress orientation and tectonic regime in the northwestern Valencia Trough from borehole data, *Tectonophysics*, *300*, 63–77.

Serpelloni, E., G. Vannucci, S. Pondrelli, A. Argnani, G. Casula, M. Anzidei, P. Baldi, and P. Gasperini (2008), Kinematics of the Western Africa–Eurasia plate boundary from focal mechanisms and GPS data, *Geophys. J. Int.*, *169*, 1180–1200.

Sibuet, J.-C., P. H. Srivastava, and W. Spakman (2004), Pyrenean orogeny and plate kinematics, *J. Geophys. Res.*, *109*, B08104, doi:10.1029/2003JB002514.

Simón-Gómez, J. L. (2004), La tectónica extensional neógena-cuaternaria en la Cordillera Ibérica, in *Geología de España*, edited by J. A. Vera, pp. 614–616, Geol. de Esp. (SGE-IGME), Madrid.

Srivastava, S. P., W. R. Roest, L. C. Kovacs, G. Oakey, S. Levesque, J. Verhoef, and R. Macnab (1990), Motion of Iberia since the Late Jurassic: Results from detailed aeromagnetic measurements in the Newfoundland Basin, *Tectonophysics.*, *184*, 229–260.

Stich, D., C. J. Ammon, and J. Morales (2003), Moment tensor solutions for small and moderate earthquakes in the Ibero-Maghreb region, *J. Geophys. Res.*, *108*(B3), 2148, doi:10.1029/2002JB002057.

Stich, D., F. Mancilla, D. Baumont, and J. Morales (2005a), Source analysis of the Mw 6.3 2004 Al Hoceima earthquake (Morocco) using regional apparent source time functions, *J. Geophys. Res.*, *110*, B06306, doi:10.1029/2004JB003366.

Stich, D., F. Mancilla, and J. Morales (2005b), Crust-mantle coupling in the Gulf of Cadiz (SW-Iberia), *Geophys. Res. Lett.*, *32*, L13306, doi:10.1029/2005GL023098.

Stich, D., E. Serpelloni, F. L. Mancilla, and J. Morales (2006), Kinematics of the Iberia–Maghreb plate contact from seismic moment tensors and GPS observations, *Tectonophysics*, *426*, 295–317, doi:10.1016/j.tecto.2006.08.004.

Vasseur, G., A. Etchecopar, and H. Philip (1983), Stress state inferred from multiple focal mechanism, *Ann. Geophys.*, *1*, 291–297.

Vázquez, J. T., and R. Vegas (2000), Acomodación de la convergencia entre África y la Península Ibérica, Golfo de Cádiz y Mar de Alborán, a partir de del análisis de terremotos, *Geogaceta*, *27*, 171–174.

Vegas, R. (1992), Sobre el tipo de deformación distribuida en el contacto entre África y la Península ibérica, *Fis. Tierra*, *4*, 41–56.

Vegas, R., G. de Vicente, A. Muñoz-Martín, A. Olaiz, A. Palencia, and M. L. Osete (2005), Was the Iberian Plate moored to Africa during the Tertiary?, *Geophys. Res. Abstr.*, *7*, 06769.

Wallace, R. E. (1951), Geometry of shearing stress and relation to faulting, *J. Struct. Geol.*, *59*, 118–130.

Ziegler, P. A. (1988), Evolution of the Arctic-North-Atlantic and the western Tethys, *Mem. Am. Assoc. Pet. Geol.*, *43*, 1–198.

Zitellini, N., M. Rovere, P. Terrinha, F. Chierici, and L. Matias (2004), Neogene through quaternary tectonic reactivation of SW Iberian passive margin, *Pure Appl. Geophys.*, *161*, 565–587.

Zoback, M. L. (1992), First- and second-order patterns of stress in the lithosphere: The World Stress Map Project, *J. Geophys. Res.*, *97*, 11,703–11,728.

Zoback, M. L., et al. (1989), Global patterns of tectonic stress, *Nature*, *341*, 291–298.

S. Cloetingh, Faculty of Earth and Life Sciences, Vrije Universiteit Amsterdam, NL-1081 HV Amsterdam, Netherlands. (sierd.cloetingh@falw.vu.nl)

G. de Vicente, J. Fernández-Lozano, A. Muñoz-Martín, A. Olaiz, and R. Vegas, Grupo de Investigación en Tectonofísica Aplicada, Departamento Geodinámica, Universidad Complutense de Madrid, ES-28040 Madrid, Spain. (gdv@geo.ucm.es; javier.fernandez@geo.ucm.es; amunoz@geo.ucm.es; ajolaizc@geo.ucm.es; ruidera@geo.ucm.es)

D. Stich, Sezione di Bologna, Istituto Nazionale di Geofisica e Vulcanologia, I-40128, Bologna, Italy. (daniel@bo.ingv.it)

J. Galindo-Zaldívar, Departamento Geodinámica, Universidad de Granada, ES-18071 Granada, Spain. (jgalindo@ugr.es)